The bright Type IIP SN 2009bw, showing signs of interaction *

C. Inserra[1,2,3]†, M. Turatto[4], A. Pastorello[5,6], M.L. Pumo[6,7], E. Baron[3,8], S. Benetti[6], E. Cappellaro[6], S.Taubenberger[9], F. Bufano[2,6], N. Elias-Rosa[10], L. Zampieri[6], A. Harutyunyan[11], A. S. Moskvitin[12], M. Nissinen[13], V. Stanishev[14], D. Y. Tsvetkov[15], V.P. Hentunen[13], V.N. Komarova[12], N.N. Pavlyuk[15], V.V. Sokolov[12], T.N. Sokolova[12].

[1]*Dipartimento di Fisica ed Astronomia, Universita' di Catania, Sezione Astrofisica, Via S.Sofia 78, 95123, Catania, Italy*
[2]*INAF Osservatorio Astrofisico di Catania, Via S.Sofia 78, 95123, Catania, Italy*
[3]*Department of Physics and Astronomy, University of Oklahoma, Norman, OK 73019*
[4]*INAF Osservatorio Astronomico di Trieste, Via Tiepolo 11, 34143, Trieste, Italy*
[5]*Astrophysics Research Centre, School of Mathematics and Physics, Queen's University Belfast, Belfast BT7 1NN, United Kingdom*
[6]*INAF Osservatorio Astronomico di Padova, Vicolo dell'Osservatotio 5, 35122, Padova, Italy*
[7]*Dipartimento di Astronomia, Universita' di Padova, Vicolo dell'Osservatorio 3, 35122, Padova, Italy*
[8]*Hamburger Sternwarte, Gojenbergsweg 112, 21029 Hamburg, Germany*
[9]*Max-Planck-Institut für Astrophysik, Karl-Schwarzschild-Str. 1, 85741 Garching, Germany*
[10]*Institut de Cincies de l'Espai (IEEC-CSIC), Campus UAB, 08193 Bellaterra, Spain*
[11]*Fundación Galileo Galilei-INAF, Telescopio Nazionale Galileo, Rambla José Ana Fernández Pérez 7, 38712 Breña Baja, TF - Spain*
[12]*Special Astrophysical Observatory of the Russian AS, Nizhnij Arkhyz 369167, Russia*
[13]*Taurus Hill Observatory, Kangaslampi, Finland*
[14]*CENTRA - Instituto Superior Tecnico, Av. Rovisco Pais, 1,1049-001 Lisbon, Portogual*
[15]*Sternberg Astronomical Institute of Lomonosov Moscow State University, University Ave., 13, 119992 Moscow, Russia*

ABSTRACT

We present photometry and spectroscopy of the type IIP supernova 2009bw in UGC 2890 from few days after the outburst to 241 days. The light curve of SN 2009bw during the photospheric phase is similar to that of normal SNe IIP but with brighter peak and plateau ($M_R^{max} = -17.82$ mag, $M_R^{plateau} = -17.37$ mag). The luminosity drop from the photospheric to the nebular phase is one of the fastest ever observed, ~ 2.2 mag in about 13 days. The radioactive tail of the bolometric light curve indicates that the amount of ejected ^{56}Ni is ≈ 0.022 M$_\odot$. The photospheric spectra reveal high velocity lines of Hα and Hβ until about 105 days after the shock breakout, suggesting a possible early interaction between the SN ejecta and pre-existent circumstellar material, and the presence of CNO elements. By modeling the bolometric light curve, ejecta expansion velocity and photospheric temperature, we estimate a total ejected mass of $\sim 8-12$M$_\odot$, a kinetic energy of ~ 0.3 foe and an initial radius of $\sim 3.6 - 7 \times 10^{13}$ cm.

Key words: supernovae: general – supernovae: individual: SN 2009bw – galaxies: individual UGC 2890 – supernovae: circumstellar interaction

1 INTRODUCTION

Type II Supernovae (SNe) are produced by the explosion following the gravitational collapse of massive stars ($M_{ZAMS} \gtrsim 7-8 M_\odot$, for details see Pumo et al. 2009; Smartt et al. 2009; Heger et al. 2003, and reference therein).
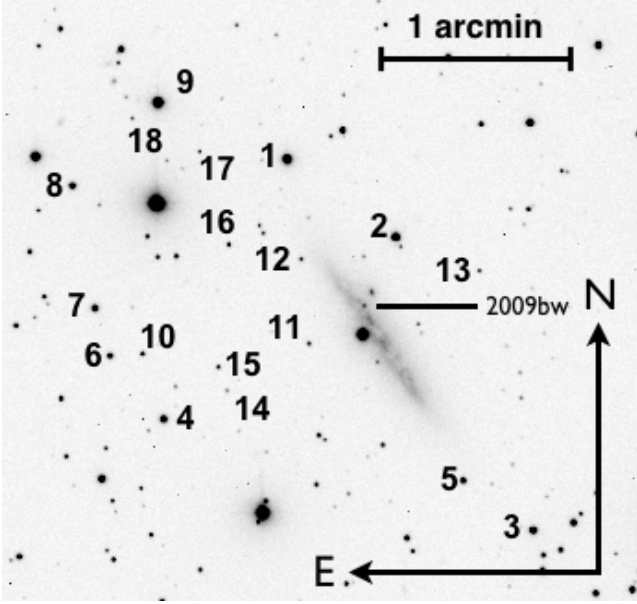
Figure 1. R band image of SN 2009bw in UGC 2890 obtained with the Calar Alto 2.2m Telescope+CAFOS (see Tab. 1) on August 30th, 2009. The sequence of stars used to calibrate the optical and NIR magnitudes of SN 2009bw is indicated.

Those retaining part of their H envelope at the time of the explosion are called type II and, if they show a constant luminosity for a period ranging from about 30 days to a few months, are assigned to the "Plateau" subclass (SNe IIP). Others present a steeper decline over the same period and are named "Linear" (SNe IIL; Barbon, Ciatti, & Rosino 1979). A third sub-class shows a slow decline and narrow emission lines in the spectra, and hence forms the so called group of "narrow" type II SNe (SNe IIn, Schlegel 1990). SNe IIP have been the subject of extensive analysis by Hamuy (2003) who pointed out a continuity in their properties and revealed several relations linking the observables to physical parameters. An independent analysis, extending the sample to low- and high-luminosity SNe IIP confirmed these results (Pastorello 2003) . Thanks to the direct identification of several SN precursors in deep pre-explosion images, recent studies support the idea that most SNe IIP are originated from explosions of stars with $M \lesssim 16\text{-}17\ M_\odot$ (Smartt et al. 2009) and are usually associated with red supergiant progenitors (Smartt 2009). Such stars have "extended", massive ($\gtrsim 5-7$ $M_\odot$) hydrogen envelopes at the time of explosion. Variation in the explosion configurations (e.g. envelope mass, energy, radius, etc.) are thought to be responsible for the relatively "large" variety of objects.

The configuration of the exploding stars and of the circumstellar matter (CSM), governed by the mass loss during the late evolutionary stages of the progenitor, can lead to different observables starting from stars of similar initial mass. Detailed studies at many different wavelengths show an almost unlimited variety of interaction scenarios between ejecta of different mass and CSM of various densities and distances from the exploding stars. As a recent example, SN 2007od (Inserra et al. 2011) shows evidence of weak interaction at early time and strong interaction at late times.

SN 2009bw is a good opportunity to explore the zoo of type IIP with early, weak interaction. It was discovered in UGC 2890 on 2009 March 27.87 UT (Nissinen, Heikkinen & Hentunen 2009). Stanishev, Adamo, & Micheva (2009) classified it as a normal type II SN soon after explosion, showing a spectrum with narrow Hα emission superimposed on a broader base.

The coordinates of SN 2009bw have been measured on our astrometrically calibrated images: $\alpha = 03^h56^m06^s.92$ $\pm0^s.05$ $\delta = +72^o55'40".90$ $\pm0."05$ (J2000). The object is located in the inner region of the highly (i=90, LEDA) inclined UGC 2890, 11" East and 22" North of the center of the galaxy (Fig. 1). This corresponds to a projected distance of ∼2.4 Kpc from the nucleus assuming a distance to UGC 2890 of ∼20 Mpc (see Sect. 2.3).

In this paper we present and discuss optical and near-infrared observations of SN 2009bw from March 2009 to August 2010. In Sect. 2 we describe the photometric observations and give details on the reduction process, the reddening estimate and the photometric evolution. In Sect. 3 we describe and analyze the spectroscopic data. The explosion and progenitor parameters retrieved through the models are presented in Sect. 4. Discussion and conclusions follow in Sect. 5 and 6.

2   PHOTOMETRY

The optical photometric monitoring of SN 2009bw started on March 30th, 2009, the day after the discovery, and continued until late November 2009. We attempted to recover the object at late time after the seasonal gap but the object was already fainter than our instrument detection limit.

2.1   Data

Ground based optical photometry was obtained with several telescopes (Tab. 1). Note that the u, r and i magnitudes of the Sloan filters of the LT and the *i*-band filter of the NOT have been reported in the Johnson–Cousin system. Optical data were reduced following standard procedures in the IRAF[1] environment. Instrumental magnitudes were measured on the final images, obtained after removal of the detector signature including overscan correction, bias subtraction, flat field correction and trimming.

Photometric zero points and colour terms were computed for all nights through observations of Landolt standard fields (Landolt 1992). Thirteen of the forty-nine nights were photometric. Using the photometry of these nights we calibrated the magnitudes of a local stellar sequence shown in Fig. 1. Magnitudes of the local sequence stars are reported in Tab. 2 along with their root mean square (r.m.s., in brackets). Finally, the average magnitudes of the local sequence stars were used to calibrate the photometric zero points obtained in non-photometric nights. The sequence extends from bright (V=13.3) to faint (V=19.4) stars to allow
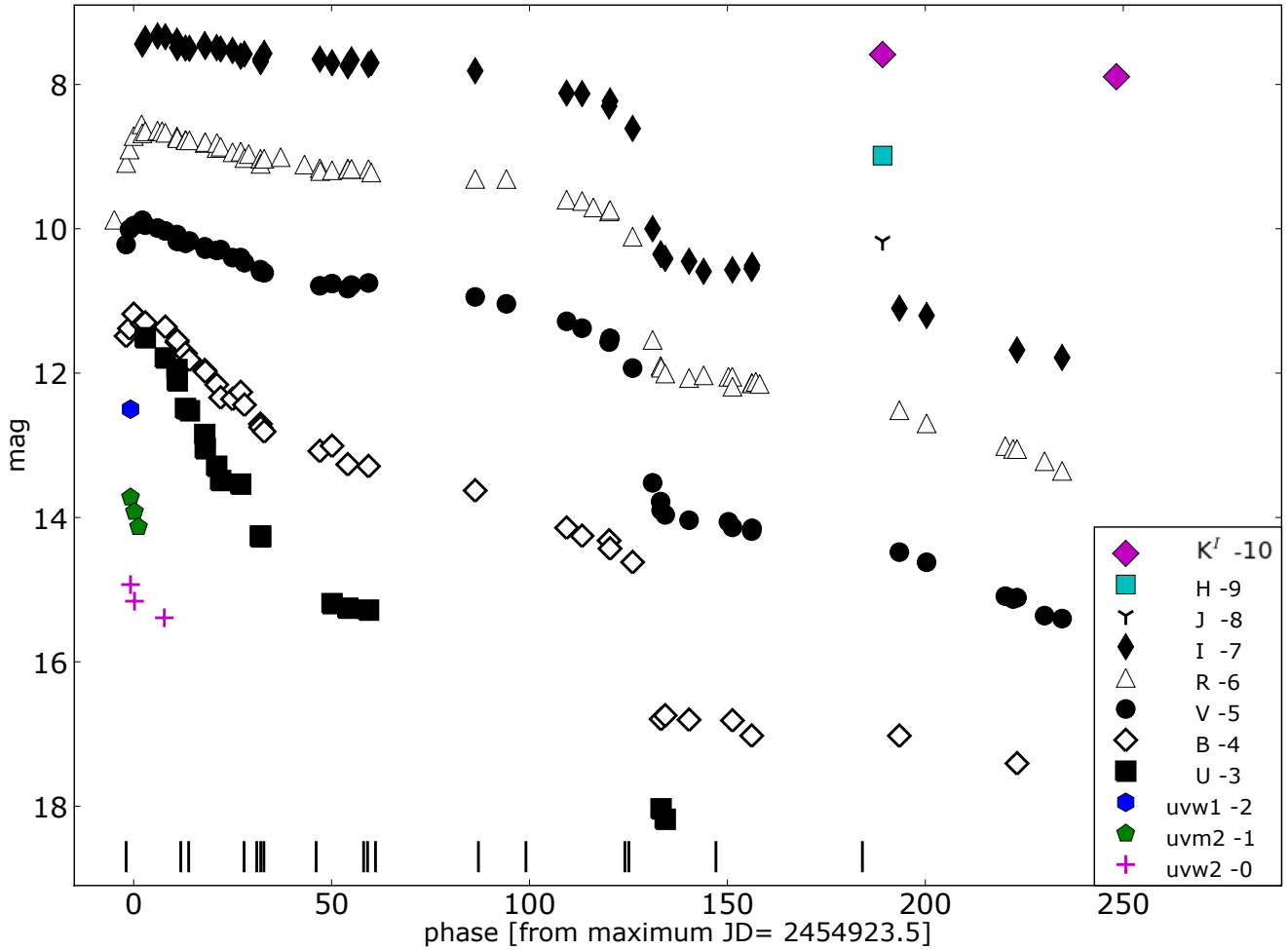
Figure 2. Synoptic view of the light curves of SN 2009bw in all available bands. The shifts from the original values reported on Tab. 3 are in the legend. Vertical marks at the bottom indicate the epochs of available spectra (cfr. Tab. 8).

a good calibration of the SN magnitudes from the luminous peak to the nebular phase. The brightest stars of the sequence were saturated on long-exposure frames with larger telescopes. Their calibration is based, therefore, on a fewer photometric nights. The calibrated optical magnitudes of the SN are reported in Tab. 3. The discovery magnitude reported in Nissinen, Heikkinen & Hentunen (2009) has been revised and reported in Tab. 3. There is no evidence of the SN presence on images obtained on August 24, 2010; the values in Tab. 3 are upper limits computed with artificial stars placed close to SN position. These values are not shown in Fig. 2 because they do not impose tight limits to the late phase decline.

Because of the complex background SN magnitudes have been evaluated in two ways: a) through the point spread function (PSF) fitting technique; b) with the template subtraction and subsequent PSF fitting technique. The magnitudes calculated with both methods during the plateau period result in good agreement. However, the results differ up to 0.5 mag during the radioactive tail phase (especially in bluer bands), and preference has been given to the reduction via the template subtraction. The values reported in Tab. 3 after June 26th have been obtained by

the latter technique. The uncertainties reported in Tab. 3 were estimated by combining in quadrature the errors in the photometric calibration and the error in the PSF fitting through artificial stars.

Near infrared (NIR) photometry was obtained at two epochs with NICS (cfr. Tab. 1) mounted at the 3.5m Telescopio Nazionale Galileo (TNG). The NIR images of the SN field were obtained combining several, sky-subtracted, dithered exposures. Photometric calibration was achieved relative to 2MASS photometry of the same local sequence stars as used for the optical calibration. The NIR magnitudes of SN 2009bw are listed in Tab. 4.

Ultraviolet (uvw2,uvm2,uvw1; see Poole et al. 2008) observations, obtained by UVOT on board of the SWIFT satellite are available for four epochs in a period of 9d. We reduced these data using the HEASARC[2] software. For each epoch all images were co-added, and then reduced following the guidelines presented by Poole et al. (2008). Aperture magnitudes are reported on Tab. 5.

Table 1. Instrument setup used for the photometric follow up.

Telescope	Primary mirror m	Camera	Array	CCD	pixel scale arcsec/pix	field of view arcmin	filters
Copernico	1.82	AFOSC	1024 x 1024	TK1024AB	0.46	8.1	Bessell B V R, Gunn i
TNG	3.58	DOLORES	2048 x 2048	EEV 42-40	0.25	8.6	Johnson U B V, Cousins R I
		NICS	1024 x 1024	HgCdTe Hawaii	0.25	4.2	J H K′
LT	2.0	RATcam	2048 x 2048	EEV 42-40	0.13	4.6	Sloan u, Bessell B V, Sloan r i
NOT	2.5	ALFOSC	2048 x 2048	EEV 42-40	0.19	6.4	Johnson U B V R, interference i
CAHA	2.2	CAFOS	2048 x 2048	SITe	0.53	16	Johnson U B V R I
SWIFT	0.3	UVOT	2048 x 2048	microchannel intensified CCD	0.48	17	uvw2,uvm2,uvw1
SAO-RAS	1.0	CCD phot.	530 x 580	EEV 42-40	0.48	2.38 x 3.53	Johnson U B V, Cousins R I
THO	0.4	ST-8XME	1530 x 1020	KAF-1603ME	0.9	24 x 16	Johnson B V, Cousins R
S50	0.5	ST-10XME	2184 x 1472	KAF-3200ME	1.12	20.6 x 13.9	Johnson V, Cousins R I
M70	0.7	Apogee AP-7p	512 x 512	SITe	0.64	5.5	Johnson U B V I, Cousins R
C60	0.6	Apogee AP-47p	1024 x 1024	EEV47-10	0.71	6.1	Johnson B V I, Cousins R
C50	0.5	Meade Pictor416	765 x 510	KAF-0400	0.92	11.7 x 7.8	Johnson V, Cousins R

Copernico = Copernico Telescope (Mt. Ekar, Asiago, Italy); TNG = Telescopio Nazionale Galileo (La Palma, Spain); LT = Liverpool Telescope (La Palma, Spain); NOT = Nordic Optical Telescope (La Palma, Spain); CAHA = Calar Alto Observatory 2.2m Telescope (Sierra de los Filabres, Andalucia, Spain); SWIFT orbiting telescope by NASA; SAO-RAS = Special Astrophysical Observatory 1m Telescope (Mt. Pastukhov, Russia); THO = Taurus Hill Observatory (Hill Härkämäki, Finland); S50 = 0.5m Newton Telescope (Tatranska Lomnica, Slovakia); M70 = 0.7m Cassegrain Telescope (Moscow, Russia); C60 = 0.6m Cassegrain Telescope (Observatory of Sternberg Astronomical Institute, Nauchnyi, Crimea); C50 = 0.5m Matsukov Telescope Meniscus (Observatory of SAI, Nauchnyi, Crimea).

Table 2. Magnitudes of the local sequence stars in the field of SN 2009bw (cfr. Fig. 1). The errors are reported in brackets

ID	U	B	V	R	I
1	14.48 (.03)	14.41 (.02)	13.73 (.01)	13.36 (.01)	12.97 (.01)
2	16.60 (.03)	15.64 (.02)	14.47 (.02)	13.83 (.01)	13.23 (.01)
3	16.21 (.02)	15.97 (.02)	15.15 (.01)	14.64 (.01)	14.15 (.01)
4	17.01 (.02)	16.42 (.02)	15.41 (.01)	14.85 (.01)	14.27 (.01)
5	17.92 (.02)	17.36 (.02)	16.34 (.01)	15.79 (.02)	15.21 (.02)
6	17.48 (.02)	17.02 (.02)	16.12 (.02)	15.61 (.02)	15.10 (.03)
7	16.60 (.02)	16.46 (.02)	15.68 (.01)	15.24 (.01)	14.78 (.01)
8	16.23 (.02)	16.22 (.02)	15.54 (.01)	15.17 (.02)	14.75 (.01)
9	15.13 (.02)	14.39 (.02)	13.27 (.02)	12.70 (.02)	12.05 (.01)
10	18.04 (.01)	17.73 (.02)	16.86 (.02)	16.45 (.01)	16.01 (.02)
11	18.90:	18.86 (.03)	18.07 (.02)	17.64 (.02)	17.24 (.02)
12		19.85 (.02)	18.40 (.02)	17.39 (.01)	16.57 (.01)
13	19.27:	19.22 (.02)	18.50 (.03)	17.99 (.02)	17.59 (.02)
14		19.98 (.02)	19.07 (.03)	18.62 (.02)	18.13 (.03)
15	18.55:	18.76 (.02)	17.94 (.02)	17.55 (.01)	17.09 (.02)
16	18.80:	18.65 (.01)	17.59 (.02)	17.00 (.01)	16.45 (.01)
17	20.46:	19.51 (.03)	18.47 (.02)	17.82 (.02)	17.26 (.02)
18		20.94 (.02)	19.36 (.03)	18.34 (.02)	17.52 (.02)

In Sect. 5 we will discuss also the implications of an 8 ksec exposure obtained with Swift-XRT which has provided an upper limit of 7.9×10^{-14}erg cm^{-2} s^{-1} (over the energy range 0.3-10 KeV) in an aperture of 9 XRT pixels ($\sim$21") centered at the position of SN 2009bw.

2.2 Photometric evolution

In Fig. 2 the *uvw2,uvm2,uvw1,U,B,V,R,I,J,H,K′* light curves of SN 2009bw are plotted. The B-, V-, I- and more clearly

R-band light curves show a slow rise to the peak, estimated to be occurred around the JD 2454923.5±1.0 in the B band. It is likely that thus the discovery of the SN happened close to the shock breakout. The early discovery is also consistent with the phases derived for the first spectra of SN 2009bw as deduced from the comparison of the early spectra with a library of supernova spectra performed with the "GELATO" code (Harutyunyan et al. 2008). Therefore, hereafter we will adopt JD 2454916.5±3 (March 25.0 UT) as an estimate for the epoch of shock breakout.

An initial slow decline of $\sim$30d, during which the SN decreases by about 0.5 mag in the V and R bands, is followed by a plateau lasting for 50 d to 100 d. The plateau is flat from V to I ($m_R \sim 15.0$, i.e. $M_R \sim -17.4$, cfr. Sect. 2.3), possibly shorter and inclined in blue bands. The plateau luminosity of SN 2009bw is more luminous than that of common SNe IIP (more than 1 mag, see Patat et al. 1994; Richardson et al. 2002) and similar to those of SNe 1992H (Clocchiatti et al. 1996), 2004et (Maguire et al. 2010) and 2007od (Inserra et al. 2011).

As shown in Fig. 2, after $\sim$110d *BVRI* light curves show a decline from the plateau. Though very fast ($\sim$2.2 mag in only 13d) the jump is less pronounced than in other SNe IIP e.g. 6 mag in SN 2007od (Inserra et al. 2011), >3.5 mag in SN 1994W (Sollerman, Cumming, & Lundqvist 1998), 3.6 mag in the low luminosity SN 2005cs (Pastorello et al. 2009).

After the drop, the light curve settles onto the radioactive tail. The late time decline rates in various bands are reported in Tab. 6. Although with some variations, these share an overall similarity with those of most SNe IIP (e.g. Turatto et al. 1990; Patat et al. 1994) and are close to 0.98 mag $(100d)^{-1}$, the decay rate of ^{56}Co to ^{56}Fe (corresponding to a lifetime of 111.26d).

In Fig. 3 we show the time evolution of the B − V and

Table 3. UBVRI magnitudes of SN 2009bw and assigned errors in brackets.

Date yy/mm/dd	JD (+2400000)	U	B	V	R	I	Inst.
09/03/27	54918.42				15.88 (.02)		7
09/03/30	54921.40		15.49 (.02)	15.22 (.01)	15.09 (.01)		6
09/03/31	54922.24		15.38 (.02)	15.01 (.01)	14.90 (.01)		6
09/04/01	54923.32		15.18 (.01)	14.96 (.01)	14.72 (.01)		7
09/04/03	54925.31				14.55 (.02)		7
09/04/03	54925.50		15.32 (.10)	14.88 (.06)	14.68 (.01)	14.44 (.02)	6
09/04/04	54926.24	14.51 (.05)	15.30 (.05)	14.95 (.02)	14.65 (.01)	14.37 (.03)	9
09/04/07	54929.33			14.99 (.02)	14.64 (.02)	14.33 (.01)	8
09/04/08	54930.46				14.65 (.07)		7
09/04/09	54931.30	14.79 (.07)	15.36 (.03)	15.03 (.02)	14.67 (.02)	14.34 (.03)	9
09/04/12	54934.25	14.95 (.15)	15.57 (.05)	15.08 (.05)	14.72 (.03)	14.40 (.03)	9
09/04/12	54934.31	15.11 (.03)	15.55 (.02)	15.18 (.02)	14.74 (.02)	14.49 (.02)	1
09/04/14	54936.40	15.49 (.02)	15.73 (.02)	15.20 (.02)	14.77 (.02)	14.50 (.02)	2
09/04/14	54936.45				14.77 (.18)		7
09/04/15	54937.39	15.52 (.02)	15.82 (.02)	15.17 (.01)	14.78 (.02)	14.50 (.02)	4
09/04/19	54941.26	15.85 (.11)	15.96 (.03)	15.25 (.02)	14.81 (.02)	14.45 (.03)	9
09/04/19	54941.39	16.05 (.02)	15.98 (.02)	15.28 (.02)	14.80 (.02)	14.48 (.02)	4
09/04/22	54944.28	16.29 (.13)	16.16 (.05)	15.30 (.03)	14.88 (.02)	14.49 (.03)	9
09/04/22	54944.34				14.81 (.01)		7
09/04/23	54945.28	16.49 (.03)	16.34 (.05)	15.29 (.02)	14.86 (.02)	14.51 (.02)	6
09/04/26	54948.28		16.36 (.04)	15.40 (.03)	14.94 (.02)	14.53 (.03)	9
09/04/28	54950.34	16.54 (.19)	16.26 (.10)	15.40 (.20)	14.93 (.12)	14.61 (.12)	1
09/04/29	54951.29		16.44 (.04)	15.47 (.03)	15.02 (.02)	14.58 (.02)	9
09/04/30	54952.38				14.97 (.25)		7
09/05/03	54955.33	17.27 (.03)	16.70 (.02)	15.57 (.02)	15.03 (.02)	14.65 (.02)	1
09/05/03	54955.38	17.26 (.04)	16.75 (.02)	15.60 (.02)	15.10 (.04)	14.69 (.02)	3
09/05/04	54956.28		16.81 (.06)	15.61 (.04)	15.03 (.03)	14.57 (.03)	9
09/05/08	54960.44				15.01 (.13)		7
09/05/14	54966.45				15.11 (.05)		7
09/05/18	54970.34		17.08 (.07)	15.79 (.03)	15.16 (.03)	14.65 (.03)	9
09/05/18	54970.44				15.20 (.15)		7
09/05/21	54973.42	18.19 (.15)	17.01 (.05)	15.76 (.02)	15.19 (.02)	14.70 (.03)	5
09/05/25	54977.39	18.26 (.19)	17.27 (.04)	15.83 (.02)	15.17 (.02)	14.74 (.02)	5
09/05/25	54977.42				15.17 (.30)		7
09/05/26	54978.33			15.78 (.15)	15.17 (.10)	14.66 (.15)	9
09/05/30	54982.63	18.28 (.09)	17.29 (.02)	15.75 (.02)	15.17 (.02)	14.73 (.02)	1
09/05/31	54983.32				15.22 (.15)	14.70 (.16)	9
09/06/26	55009.58		17.63 (.02)	15.94 (.02)	15.31 (.02)	14.82 (.02)	1
09/07/04	55017.46			16.04 (.15)	15.31 (.12)		10
09/07/19	55032.68		18.15 (.04)	16.29 (.02)	15.60 (.02)	15.12 (.02)	3
09/07/23	55036.58		18.26 (.08)	16.38 (.02)	15.62 (.02)	15.13 (.02)	5
09/07/26	55039.43				15.71 (.05)		7
09/07/30	55043.42		18.32 (.17)	16.57 (.10)	15.76 (.10)	15.30 (.10)	9
09/07/30	55043.65		18.43 (.03)	16.52 (.03)	15.74 (.03)	15.23 (.03)	1
09/08/05	55049.35		18.62 (.30)	16.93 (.10)	16.11 (.10)	15.61 (.10)	9
09/08/10	55054.40			18.52 (.30)	17.54 (.16)	17.00 (.15)	9
09/08/12	55056.43			18.78 (.20)	17.90 (.18)	17.35 (.30)	9
09/08/12	55056.54	20.04 (.40)	20.79 (.09)	18.90 (.10)	17.93 (.06)	17.36 (.08)	1
09/08/13	55057.59	21.18 (.38)	20.74 (.09)	18.96 (.12)	18.01 (.04)	17.41 (.07)	2
09/08/20	55063.61		20.80 (.21)	19.23 (.11)	18.12 (.17)	17.47 (.13)	5
09/08/23	55067.29				18.03 (.15)	17.59 (.30)	9
09/08/29	55073.55			19.06 (.15)	18.05 (.10)		11
09/08/30	55074.52				18.05 (.15)		11
09/08/30	55074.57		20.81 (.04)	19.14 (.13)	18.19 (.08)	17.57 (.08)	1
09/09/04	55079.44		21.02 (.05)	19.19 (.04)	18.14 (.04)	17.55 (.07)	1
09/09/04	55079.53			19.15 (.16)	18.14 (.12)	17.51 (.27)	11
09/09/05	55080.47				18.12 (.12)		11
09/09/06	55081.43				18.15 (.12)		11
09/10/12	55116.74		21.03 (.11)	19.48 (.29)	18.51 (.57)	18.10 (.15)	3
09/10/18	55123.62			19.62 (.13)	18.70 (.11)	18.20 (.12)	5
09/11/07	55143.50			20.09 (.27)	19.01 (.15)		11
09/11/09	55145.47			20.13 (.21)	19.05 (.18)		11
09/11/10	55146.46		21.41 (.12)	20.11 (.19)	19.05 (.56)	18.68 (.22)	3
09/11/17	55153.42			20.36 (.21)	19.22 (.12)		11
09/11/22	55157.85			20.40 (.21)	19.36 (.24)	18.78 (.25)	1
10/08/24	55433.69			> 21.9	> 20.3	> 19.5	3

1 = CAHA, 2 = NOT, 3 = TNG, 4 = LT, 5 = Copernico, 6 = SAO-RAS, 7 = THO, 8 = S50, 9 = M70, 10 = C50, 11 = C60. The telescopes abbreviations are the same of Tab. 1.

V − I colour curves of SN 2009bw together with those of SNe 1987A, 2005cs, 2004et, 1999em and 2007od, dereddened according to the values of Tab. 7.

All typical SNe IIP show a similar colour evolution with a rapid increase of B–V as the SN envelope expands and cools. After about 40d the colour changes more slowly as the rate of cooling decreases. SN 2009bw follows the general behavior. The only exception to this smooth trend is SN 2005cs which shows a red jump about at 120d, that seems a characteristic of low-luminosity SNe II (Pastorello et al. 2004).
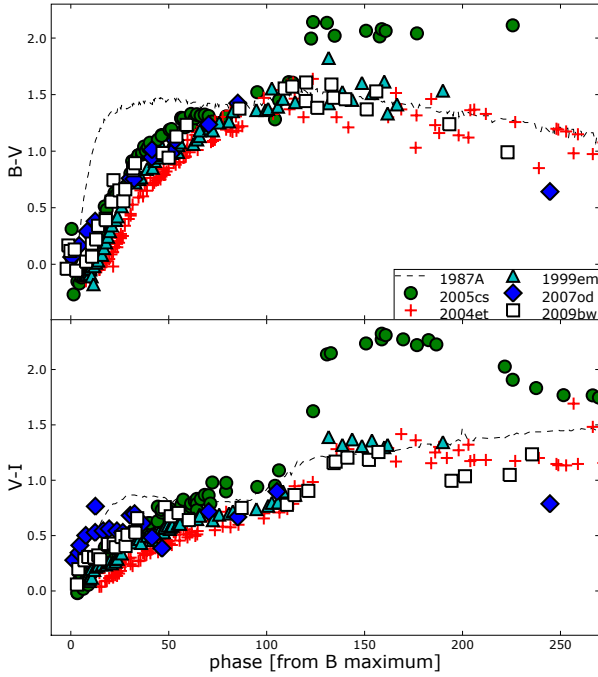
Figure 3. Comparison of the dereddened colours of SN 2009bw and those of SNe 1987A, 2005cs, 1999em, 2004et and 2007od. The phase of SN 1987A is with respect to the explosion date.

Table 6. Main data of SN 2009bw.

position (2000.0)	$03^h56^m02^s.92$	$+72^o55^m40^s.9$
parent galaxy morphology	UGC 2890, Sdm pec:	
offset wrt nucleus	$11''$E	$22''$N
adopted distance modulus	$\mu = 31.53 \pm 0.15$	
SN heliocentric velocity	1155 ± 6 km s^{-1}	
adopted reddening	E_g(B-V)= 0.23	E_{tot}(B-V)= 0.31

	peak time (JD 2454000+)	peak observed magnitude	peak absolute magnitude
B	923 ± 1	15.18 ± 0.01	-17.70 ± 0.15
V	925 ± 1	14.88 ± 0.06	-17.67 ± 0.16
R	925 ± 1	14.55 ± 0.02	-17.82 ± 0.15
I	929 ± 1	14.33 ± 0.01	-17.83 ± 0.15
UBVRI	925 ± 2	$L_{bol} = 2.6 \times 10^{42}$ erg s^{-1}	

rise to R max	~ 8 days	
explosion day	$\sim 916.5 \pm 3$	~ 25 Mar. 2009

	late time decline [mag(100d)$^{-1}$]	interval [days]
V	1.00	139–239
R	1.09	139–239
I	1.13	139–239
UBVRI(tot)	1.06	139–239
UBVRI(1seg)	0.70	139–156
UBVRI(2seg)	1.16	161–239

M(^{56}Ni)	0.022 M$_\odot$
M(ejecta)	8.3 – 12 M$_\odot$
explosion energy	0.3 $\times 10^{51}$ ergs

Table 4. JHK$'$ TNG magnitudes of SN 2009bw and assigned errors.

Date yy/mm/dd	JD (+2400000)	J	H	K$'$
09/10/07	55112.49	18.17 (.18)	17.99 (.15)	17.59 (.13)
09/12/05	55171.50			17.89 (.08)

Table 7. Main parameters of SNe II used in the comparisons with SN 2009bw.

SN	μ^*	E(B–V)	Parent Galaxy	References
1987A	18.49	0.195	LMC	1
1992H	32.38	0.027	NGC 5377	2
1998S	31.08	0.232	NGC 3877	3
1999em	29.47	0.1	NGC 1637	4,5
2004et	28.85	0.41	NGC 6946	6
2005cs	29.62	0.05	M 51	7
2006bp	31.44	0.031	NGC 3953	8
2007od	32.05	0.038	UGC 12846	9

* In the $H_0 = 73$ km s^{-1} Mpc^{-1} distance scale
REFERENCES: 1 - Arnett et al. (1989), 2 - Clocchiatti et al. (1996), 3 - Fassia et al. (2001), 4 - Elmhamdi et al. (2003), 5 - Baron et al. (2000), 6 - Maguire et al. (2010), 7 - Pastorello et al. (2009), 8 - Quimby et al. (2007), 9 - Inserra et al. (2011)

The B–V trend of SN 2009bw during the early days seems redder than that of normal SNe IIP such as SN 1999em, and closer to that of SN 2007od. The last two points suggest a blue excess, as does the SN 2007od, but the errors of these points are large and we will not consider it any further. The V–I colour evolution of SN 2009bw is similar to that of other type IIP SNe (cfr. Fig. 3).

Table 5. Swift magnitudes of SN 2009bw and assigned errors.

Date yy/mm/dd	JD (+2400000)	uvw2	uvm2	uvw1
09/04/01	54922.51	14.93 (.06)	14.72 (.07)	14.50 (.10)
09/04/02	54923.51	15.16 (.06)	14.92 (.08)	
09/04/03	54924.52		15.13 (.09)	
09/04/09	54931.05	15.39 (.06)		

2.3 Reddening and absolute magnitude

The Galactic reddening to UGC 2890 is E_g(B-V) = 0.231 mag ($A_g(B) = 0.996$ mag) according to Schlegel, Finkbeiner, & Davis (1998), a relative large value consistent with the low Galactic latitude of UGC 2890 (b_2=14°.7, LEDA). In the optical spectra of SN 2009bw the absorption features due to interstellar NaID ($\lambda\lambda$5890,5896) of the Galaxy are present, with an average EW$_g$(NaID)$\sim$1.37 Å, as determined by our best resolution spectra (cfr. Sect. 3). According to Turatto, Benetti, & Cappellaro (2003) this corresponds to a Galactic reddening E_g(B-V)$\sim$0.22 mag ($A_g(B)\sim$0.92 mag). This

is in good agreement with Schlegel, Finkbeiner, & Davis (1998). With the same method we can estimate the reddening inside the parent galaxy. Interstellar NaID components within the host galaxy have been measured with an average EW_i(NaID)~ 0.52 Å that corresponds to a low internal reddening E_i(B-V)~ 0.08 mag or A_i(B)~ 0.35 mag. We should warn the reader that recently Poznanski et al. (2011) have suggested that NaID lines in SNIa spectra are poor tracers of dust extinction. However, having no alternative throughout this paper we have adopted a total reddening E_{tot}(B-V) $= 0.31 \pm 0.03$ mag.

NED provides a heliocentric radial velocity of $v_{hel}(UGC2890) = 1155 \pm 6$ km s^{-1}. Adopting $H_0 = 73$ km s^{-1} Mpc^{-1} and a velocity corrected for the Virgo infall of $v_{Virgo} = 1473 \pm 16$ km s^{-1} (Mould et al. 2000) we obtain a distance modulus $\mu = 31.53 \pm 0.15$ mag which will be used throughout this paper. Tully et al. (2009) provided a $\mu = 30.23 \pm 0.40$ mag ($H_0 = 72$ km s^{-1} Mpc^{-1}), this would make SN 2009bw more than 1 mag fainter, however it is inconsistent with the identified galaxy lines.

Assuming the above distance and extinction values, we find $M_B^{max} = -17.72 \pm 0.15$, $M_V^{max} = -17.67 \pm 0.16$, $M_R^{max} = -17.82 \pm 0.15$ and $M_I^{max} = -17.83 \pm 0.15$, where the reported errors include the uncertainties on the adopted distance modulus, reddening and magnitude measurements.

2.4 Bolometric light curve and ^{56}Ni mass

Unfortunately, because of the lack of simultaneous optical–NIR observations it is impossible to obtain a true bolometric light curve for SN 2009bw. In fact extended coverage from B to K′ is available only in the late radioactive tail. In order to obtain the bolometric light curve, we convert only *UBVRI* broadband magnitudes (corrected for the adopted extinction, cfr. Sect. 2.3) into fluxes at the effective wavelengths and integrate them over the entire range (flux integration limits equal to zero). Flux was then converted to luminosity using the distance adopted in Sect. 2.3. The emitted flux was computed at phases in which R observations were available. When simultaneous observations in a bandpass were unavailable, the magnitudes were interpolated from the light curves using low-order polynomials, or extrapolated. The peak of the bolometric light curve is reached close to the R-band maximum on $JD_{max}^{bol} = 2454925.3 \pm 2.0$ at a luminosity $L_{bol} = 2.6 \times 10^{42}$ erg s^{-1}.

The nebular tail of the bolometric light curve declines at a rate $\gamma \sim 1.06$ mag $(100d)^{-1}$, measured from 138d–239d since explosion, which matches the decay of ^{56}Co to ^{56}Fe suggesting complete γ-ray trapping. However, we noticed that the tail can be divided into two different segments: a flatter one from 138d to 156d with $\gamma \sim 0.70$ mag $(100d)^{-1}$ resembling that of the early tail of SN 1999em and present in many SNe, and a second one (161d–239d) with $\gamma \sim 1.16$ mag $(100d)^{-1}$. The last two points at $\sim$234-240d seem to suggest a further increase of the decline rate, maybe due to dust formation. However, due to the relatively large errors this is not significant and we will not elaborate it any further.

In Fig. 5 we compare the bolometric (*UBVRI*) light curve of SN 2009bw with those of other SNe reported in Tab. 7. The early luminosity of SN 2009bw is slightly smaller than those of the luminous SNe 2007od, 2004et, 1992H. The duration of the plateau resembles those of SN 1992H and
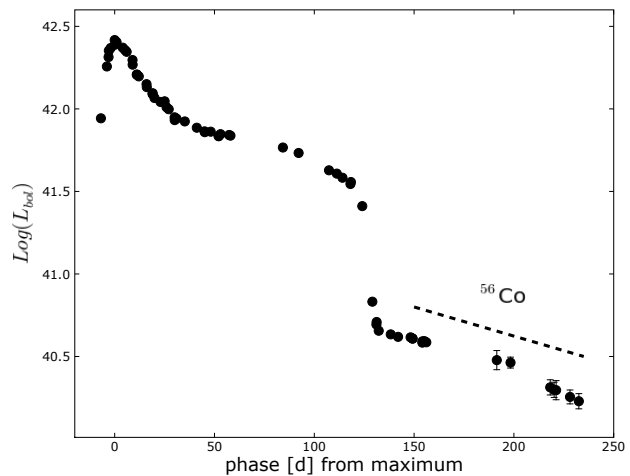

Figure 4. *UBVRI* bolometric light curve of SN 2009bw. The slope of ^{56}Co to ^{56}Fe decay is also displayed for comparison. Distance modulus and reddening are reported in Tab. 6.

SN 2004et, whilst it is longer than that of the peculiar SN 2007od. The peak seems slightly broader than those of other SNe IIP including SN 2007od. The luminosity drop from the plateau to the tail of SN 2009bw appears intermediate between the high value for 2007od and the small value for 1999em.

The ^{56}Ni mass ejected by SN 2009bw has been derived by comparing its bolometric light curve to that of SN 1987A assuming similar γ-ray deposition fraction

$$M(^{56}Ni)_{09bw} = M(^{56}Ni)_{87A} \times \frac{L_{09bw}}{L_{87A}} M_\odot \qquad (1)$$

where $M(^{56}Ni)_{87A} = 0.075 \pm 0.005$ $M_\odot$ is the mass of ^{56}Ni produced by SN 1987A (Arnett 1996), and L_{87A} is the *UBVRI* luminosity of 1987A at a comparable epoch. The comparison, performed between 161d and 205d from explosion, gives $M(^{56}Ni)_{09bw} \sim 0.022$ $M_\odot$. Indeed $L_{bol}(09bw)$ on the tail is similar to that of SN 1999em that ejected ~ 0.022 $M_\odot$ of ^{56}Ni (Elmhamdi et al. 2003). We have crosschecked this result by using the formula from Hamuy (2003) and assuming that γ-rays resulting from the ^{56}Co decay are fully thermalized at this epoch

$$M(^{56}Ni)_{09bw} = \left(7.866 \times 10^{-44}\right) L_t exp\left[\frac{(t-t_0)/(1+z)-6.1}{111.26}\right] M_\odot (2)$$

where t_0 is the explosion time, 6.1d is the half-life of ^{56}Ni and 111.26d is the *e*-folding time of the ^{56}Co decay, that release 1.71 MeV and 3.57 MeV, respectively, in the form of γ-rays (Cappellaro et al. 1997; Woosley, Hartmann, & Pinto 1989). This method provides $M(^{56}Ni)\sim 0.021$ $M_\odot$, consistent with the preceding value within the uncertainties. The single epoch (161d) of NIR observations shows a NIR contribution of $\sim$20%, which is similar to that of the other IIP SNe (see Fig.7 of Inserra et al. 2011).

Good sampling of the end of the plateau phase and the beginning of the radioactive tail allows us to estimate the steepness function S (maximum value at the transition phase of the first derivative of the plateau absolute visual magnitude) and in turn the ^{56}Ni mass using the method devised by Elmhamdi, Chugai, & Danziger (2003). We evaluated $S = 0.57$ corresponding to 0.002 $M_\odot$ of ^{56}Ni, typical of faint
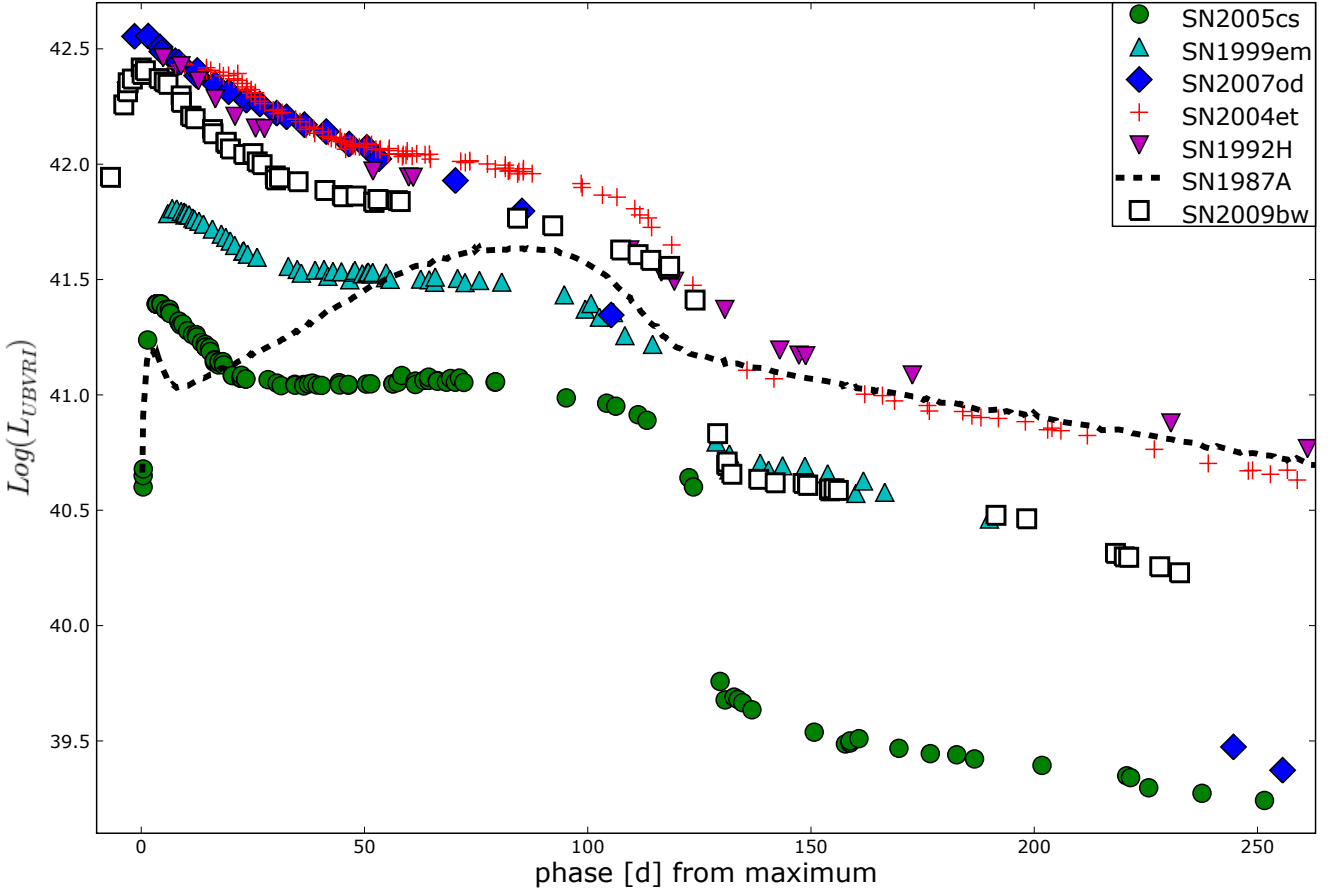
Figure 5. Comparison of bolometric (*UBVRI*) light curves of SN 2009bw with those of other Type II SNe. The distances and reddenings for the various objects are reported on Tab. 7. Small misalignments in the epoch of the maximum are due to different shifts between the maxima of the band adopted as reference and the bolometric one.

CC-SNe and very different from the previous estimates. The S value is larger than in all SNe of the sample of Elmhamdi, Chugai, & Danziger (2003) and extremely different to those of similar luminosity SNe 1992H ($S = 0.048$) and 1999em ($S = 0.118$). This result suggests that in this case the anti-correlation between steepness function and ^{56}Ni mass does not work, implying something uncommon in the high photospheric luminosity or a transition masked by some effect. We will address this issue in Sect. 5.

3   SPECTROSCOPY

The spectroscopic monitoring of SN 2009bw was carried out with several telescopes over a period of six months. The journal of spectroscopic observations is reported in Tab. 8.

3.1   Spectra reduction

Spectra were reduced (including trimming, overscan, bias correction and flat-fielding) using standard routines of IRAF. An optimal extraction of the spectra was adopted to improve the signal-to-noise rate (S/N). Wavelength calibration was performed through spectra of comparison lamps

acquired with the same configurations as the SN observations. Atmospheric extinction correction was based on tabulated extinction coefficients for each telescope site. Flux calibration was done using spectrophotometric standard stars observed with the same set-up as SN in the same nights. Absolute flux calibration was checked by comparison with the photometry, integrating the spectral flux transmitted by standard *BVRI* filters and, when necessary, adjusting it by a multiplicative factor. The resulting flux calibration is accurate to within approximately 0.1 of magnitude. The spectral resolutions in Tab. 8 were estimated from the full widths at half maximum (FWHM) of the night sky lines. We used the spectra of standard stars to remove when possible telluric features in the SN spectra. The regions of the strongest atmosphere features are marked in Fig. 6. Spectra of similar quality obtained in the same night with the same telescope have been combined to increase the S/N.

The spectrum of May 28 (64d) revealed some problems in the flux calibration of the blue side. The spectral continuum was forced to follow the spectral energy distribution (SED) derived fitting with a low order polynomial function the photometry obtained in the same night. This spectrum has not been used in the estimate of the temperature in Sect. 3.3. Since no significant evolution is expected, the spec-
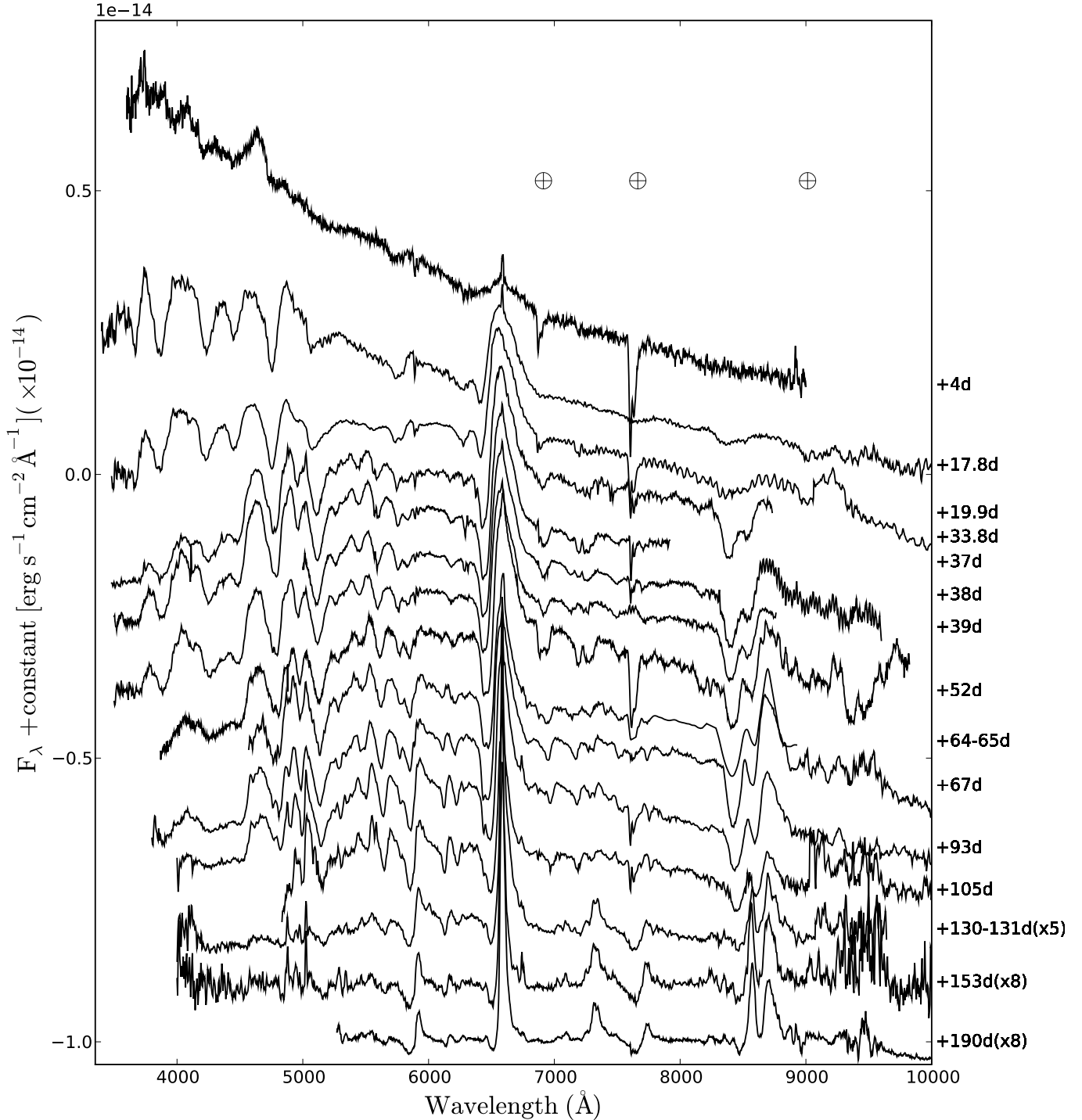
Figure 6. The overall spectral evolution of SN 2009bw. Wavelengths are in the observer rest frame. The phase reported for each spectrum is relative to the explosion date (JD 2454916.5). The ⊕ symbols mark the positions of the most important telluric absorptions. The ordinate refers to the first spectrum. The second spectrum is shifted downwards by 2×10^{-15} units, the third by 3.3×10^{-15} units with respects to the second, others by 1.5×10^{-15} erg s^{-1} cm^{-2} Å^{-1} with respect to the previous.

tra at 64d and 65d, as well as those at 130d and 131d have been combined in Fig. 6.

For SN 2009bw a single NIR spectrum was collected at a phase at 20d, which was reduced and extracted through standard routines of IRAF. As for the optical, the spectrum

was calibrated in wavelength through spectra of comparison lamps acquired with the same configuration of the SN observation. First order flux calibration was obtained using telluric A0 standard stars taken in the same night with the SN set-up. The prominent telluric bands were identified

Figure 7. Composed spectrum of SN 2009bw, from optical to NIR wavelengths, at ∼ 20d past explosion (JD 2454916.5). Wavelengths are in the observer rest frame. A black body fit at ∼7900 K is over-plotted. The regions of the strongest atmospheric features are not shown.

through the spectra of the standard star and thus removed. The combined optical and NIR spectrum on day 20 is shown in Fig. 7.

3.2　Spectra analysis

Fig. 6 shows the spectral evolution of SN 2009bw from ∼2d before maximum to over six months past peak, well sampled both in the photospheric and early nebular stages.

The first spectrum, used for classification by Stanishev, Adamo, & Micheva (2009), shows a blue continuum typical of SNe II at the same age. An unusual, prominent feature at 4600Å appears near maximum. The feature is not present in the subsequent spectrum (18d), and is most likely related to the SN since it is relatively broad (FWHM∼140Å) and has a short life. No significant emission of the underlying HII region, well seen at other wavelengths, is present in this range even in the latest spectra at 190d (N II, N III, O II and forbidden Fe III lines are present in the spectra of typical HII regions at about 4600Å, cfr. Tsamis et al. 2003). The FWHM of the 4600Å feature corresponds to a velocity v∼9100 km s^{-1}, larger than the velocity of Hα (∼7000 km s^{-1}), leading us to explore the possibility of a unusual line formation mechanism or to a very peculiar line blending. Similar features seen in ultra-luminous type Ic SNe (Pastorello et al. 2010; Quimby et al. 2011) have been identified as O II, but at wavelengths slightly bluer than this (λ4414). Concerning the opacity, its component related to the bound free process has a saw-tooth behaviour. If we consider a complex atmosphere, formed by H+He+heavy elements (e.g. Fe, Si) with temperature of the order of T∼10^4, the opacity in a window of the order of 10^2 Å around this wavelength is in a minimum with little dependence on T (Rutten 2003). In this hypothesis the emission from lines due to highly ionized elements like N III, N IV and C V is allowed. On the other hand, we can not exclude the possibility of an extreme toplighting effect (concerning a flip of the P-Cygni profile, see Branch et al. 2000) relative to Hβ and not observed in the Hα due to a difference in the optical depth (maybe due

to the interaction). However to observe this effect the interaction should be really strong while nothing in the light curve suggests such strong interaction. Actually, the comparison with SN 2006bp and SN 1998S shown in panel a) of Fig. 8 suggests the identification of this feature as a blend of highly ionized N and C. Indeed, the feature is closer in wavelength to that observed in SN 1998S, identified by Fassia et al. (2001) as CIII/NIII emission, rather than that in SN 2006bp attributed to He II λ4686 by Quimby et al. (2007). Note however that the difference between the FWHM of our feature (140Å) and the CIII/NIII of SN 1998S (∼20Å) is remarkable. The similarity with SN 1998S becomes more convincing if one compares a spectrum of 2-3 weeks after the explosion (FWHM of the blended feature ∼ 180Å, cfr. Fig. 8, panel a).

The spectra at 18d and 20d are characterized by a blue continuum, comparable to that of SN 1992H and slightly bluer than that of SN 1999em at a similar age (cfr. Fig. 8 panel b & Fig. 11). In the optical domain we identified H Balmer lines, He I 5876Å and some Fe II multiplet lines. In this set of spectra a narrow Hα emission due to an underline H II region is visible.

In order to perform a detailed line identification, we computed a synthetic photospheric spectrum model using SYNOW (Fisher 2000) and matching the properties of our observed +18d spectrum. We adopted a blackbody temperature T$_{bb}$ ∼12000 K, an expansion velocity at the photosphere v$_{phot}$ ∼7000 km s^{-1} (cfr. Sect. 3.3), an optical depth τ(v) parameterized as a power law of index $n = 9$ and an excitation temperature T$_{exc}$=10000 K, constant for all ions. The most relevant spectral features are reproduced using only 6 ions (Fig. 9). The P-Cygni profiles of the Balmer lines are clearly visible, as well as He I λ5876, but there is also contribution from Ca II, Fe II, Fe I and Si II. Detached H lines better match the line troughs. The poor fit of the Ca II IR triplet is due to low optical depth, which is however necessary to reproduce the Ca II H & K lines. We excluded the O I ion because of the early phase of the spectrum.

The line at about 6250Å has been identified as Si II λ6355 with an expansion velocity comparable to those of the other metal ions. The presence of Si II has been identified in several type II SNe, such as 2007od (Inserra et al. 2011), 2005cs (Pastorello et al. 2006), 1992H (Clocchiatti et al. 1996), 1999em (Dessart & Hillier 2005) and 1990E (Schmidt et al. 1993).

In the NIR spectrum (20d), having a photospheric temperature derived from a blackbody fit of ∼7900 K (cfr.Fig. 7) the P-Cygni profiles of the Paschen series are detected, in particular Paschen β and Paschen γ. The latter is blended with He I λ10830, and has a velocity which is higher by Δv∼2200 km s^{-1} than that of He I 5876Å.

The subsequent set of spectra (33d-39d) shows well developed P-Cygni profiles of Balmer and metal lines. Sc II λ5031 on the red side and Sc II λ4670 on the blue side of Hβ are visible, as well as the Fe II multiplet 42 lines (λλ 4924, 5018, 5169), Fe II at about 4500Å, Fe I, and Sc II in the region between 5200Å and 5500 Å. Starting from day ∼34, the He I λ5876 forms a blend with the Na ID. The Ca II IR triplet (λλ 8498, 8542, 8662) is well developed, while the H&K Ca II feature blends with Ti II. O I at about 7700Å starts to be visible. Si II λ6355 has now disappeared, and
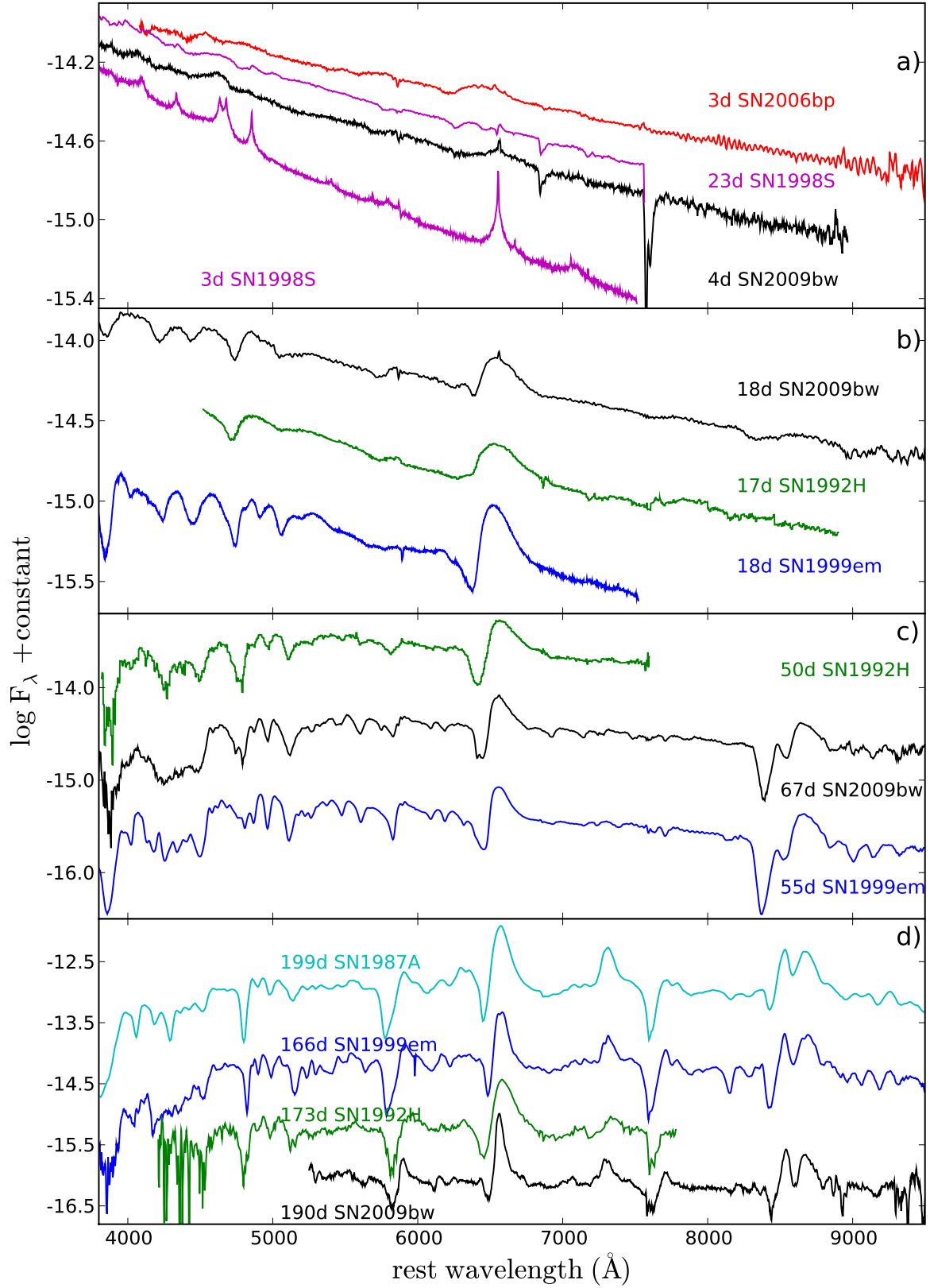
Figure 8. Panel a): comparison among spectra of SN 2009bw, SN 1998S and SN2006bp about ∼4d past explosion, plus the spectrum of SN 1998S at 23d. Panel b): comparison between spectra of SN 2009bw, SN 1999em and SN 1992H about 18d past explosion. In panel c) spectra of SN 2009bw, SN 1999em and SN 1992H in the plateau phase are compared and in panel d) spectra of SN 2009bw, SN 1987A, SN 1999em and SN 1992H during the nebular phase are shown. For references, see the text and Tab. 7, except the SN 1987A spectrum (Suntzeff & Bouchet 1990).

Table 8. Journal of spectroscopic observations of SN 2009bw.

Date	JD +2400000	Phase* (days)	Instrumental configuration	Range (Å)	Resolution[†] (Å)
09/03/29	54920.5	4.0	NOT+ALFOSC+gm4	3600-9000	13
09/04/12	54934.3	17.8	CAHA+CAFOS+b200,r200	3380-10000	10
09/04/14	54936.3	19.8	NOT+ALFOSC+gm4	3480-10000	13
09/04/15	54937.3	20.8	TNG+NICS+ij,hk	8750-24600	18,36
09/04/28	54950.3	33.8	CAHA+CAFOS+b200	3480-8730	10
09/05/01	54953.5	37.0	TNG+DOLORES+LRB	3500-7900	15
09/05/02	54954.5	38.0	TNG+DOLORES+LRR	5000-9600	15
09/05/03	54955.3	39.0	CAHA+CAFOS+b200	3500-8760	10
09/05/16	54968.5	52.0	BTA+SCORPIO+G400	3870-9830	13
09/05/28	54980.5	64.0	Copernico +AFOSC+gm4	4500-7760	25
09/05/29	54981.5	65.0	Copernico +AFOSC+gm2	5330-9020	37
09/05/31	54983.5	67.0	CAHA+CAFOS+g200	3780-10000	9
09/06/26	54509.5	93.0	CAHA+CAFOS+g200	4000-10000	10
09/07/18	55021.5	105.0	CAHA+CAFOS+g200	4800-10000	14
09/08/12	55046.5	130.0	CAHA+CAFOS+g200	4000-9650	12
09/08/13	55047.5	131.0	NOT+ALFOSC+gm4	4200-9100	18
09/09/04	55069.5	153.0	CAHA+CAFOS+g200	4000-10000	9
09/10/11	55106.5	190.0	TNG+DOLORES+LRR	5260-10000	16

* with respect to the explosion epoch (JD 2454916.5)
† as measured from the full-width at half maximum (FWHM) of the night sky lines

The abbreviations are the same of Tab. 1; in addition BTA = The 6m Big Telescope Alt-Azimutal (Mt. Pastukhova, Russia).

Figure 9. Comparison between the optical spectrum of SN 2009bw at 17.8d after the explosion (JD 2454916.5) and SYNOW synthetic spectra (for the composition of the synthetic spectra, see the text). Two models are plotted having H detached (blue dash-dotted line) or undetached (red dashed line). The observed spectrum has been corrected for extinction in the Galaxy, reported to the local restframe and normalized to its continuum. The most prominent absorptions are labelled.

the bottom of the Hα absorption shows a flat profile. We will discuss in detail the line profiles in Sect. 5.

In the late plateau phase the spectra continue to show the elements identified at earlier phases, complemented by Ba II and Ti II, whose presence indicate a temperature of ∼5000 K. Both ions are required for explaining several features between 4000 and 5000 Å. In particular, Ba II λ6142 is clearly visible. At this phase Ba I may contribute to the

blends of lines in the wavelength range 5000–6000Å, and Mg II around 9140Å.

SYNOW fairly reproduces the characteristics of the best signal-to-noise spectrum obtained in the late plateau phase (∼67d) with the following parameters: T_{bb} ∼5400 K, v_{phot} ∼3050 km s^{-1} (cfr. Sect. 3.3), optical depth $\tau(v)$ parameterized as a power law of index $n = 7$, and T_{exc}=5000–8000 K for neutral atoms and 10000 K for ionized species. The SYNOW spectrum (Fig. 10) has been obtained by considering 11 different contributing ions (red dashed line): H I, C I, N I, O I, Na I, Ca II, Sc II, Ti II, Fe I, Fe II, Ba II. The inclusion of two additional ions (blue dash-dotted line), Ba I and Mg II, allows for a better fit of the absorption on the blue wing of Na ID at 5745Å and the absorption at 9145Å as a blend of O I and Mg II. The absorption feature visible around 7100Å and poorly fitted by both the synthetic spectra could be Ti II with a different optical depth. However, because of the noise and the presence of telluric absorptions in this range it is difficult to draw a firm conclusion. The discrepancy in the emission between the SYNOW fits and observed spectra at about 4500 Å is perhaps due to a high optical depth of Ti II that masks the emission of nearby lines. Other discrepancies between observed and synthetic spectra may be attributed to NLTE effects ignored in our computation. H I and Ca II are detached to improve the line fit, but this causes problems in fitting the red wings. Interesting lines are identified on the red side (>7000Å) of the spectrum, where absorptions due to the elements of the CNO cycle appear. In particular, O I λ7774 is present, and possibly also O I λ9260, blended with Mg II. N I has been identified around 7400Å and 8130Å. C I appears around 9010Å and 9310Å and possibly around 4615Å close to the Sc II line, but in this region the fit is affected by the emission profile of detached hydrogen. O I and N I have been identified at this phase in other SNe, e.g. 1999em (Pastorello
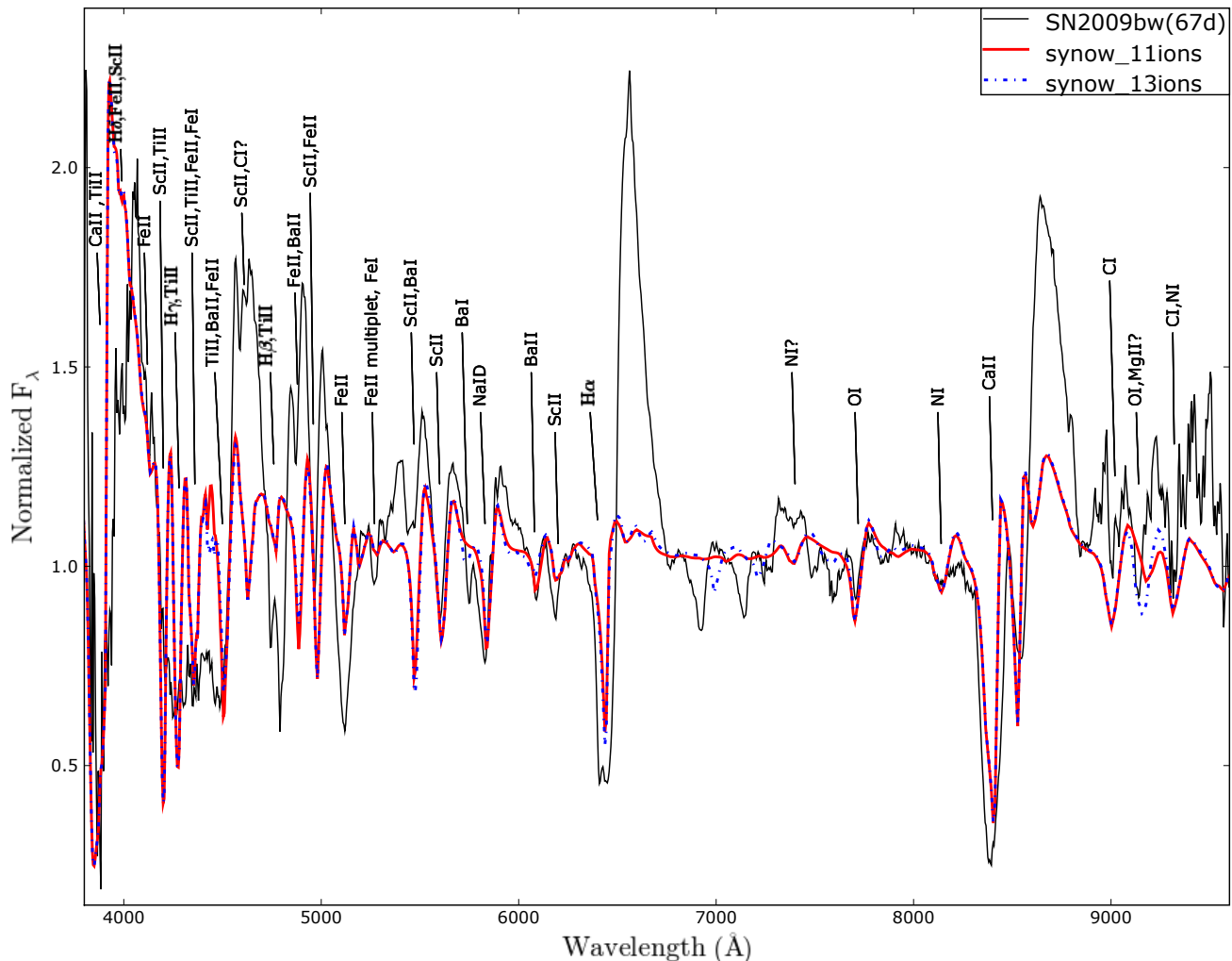
Figure 10. Comparison between the optical spectrum of SN 2009bw at ∼67d after explosion (JD 2454916.5) and two SYNOW analytical spectra. The difference between the SYNOW spectra is the presence of Ba I and Mg II ions (blue). The spectrum has been corrected for extinction in the Galaxy and reported to the SN restframe. The most prominent absorptions are labelled.

2003), but the presence of C I lines in spectra of type IIP SNe has only occasionally been claimed, e.g. in SNe 1995V (Fassia et al. 1998) and 1999em (Pastorello 2003).

Fig. 8 (panel c) shows the comparison of spectra of several SNe II in the plateau phase. The spectrum of SN 2009bw appears similar to that of SN 1992H, sharing features commonly present in SNe IIP during the plateau phase. The comparison is interesting with SN 1999em around 9000Å, where SYNOW has identified C I lines. Unfortunately the other SN 2009bw spectra do not cover this wavelength range. The flat absorption profile of Hα resembles that observed in SN 1999em. In Sect. 5 we will discuss this feature arguing that this is due to weak CSM interaction.

Three early nebular spectra of SN 2009bw have been collected between 130d and 190d. A narrow component appears at the host galaxy rest position, confirming that it is due to an underlying H II region. The broad Hα emission, attributed to the SN ejecta, is also centered at the rest wavelength and shows a residual absorption. Na ID and Ca II IR triplet absorptions are clearly visible. The spectra show also

evidence of the forbidden emission of the [Ca II] λλ7291, 7324 doublet. Compared to other SNe IIP (panel d of Fig. 8) is noticeable the complete absence of [O I] λλ6300,6363 even in the latest available SN 2009bw spectrum, and the relatively narrow FWHM of the emission lines (FWHM(Hα) ∼1900 km s^{-1}).
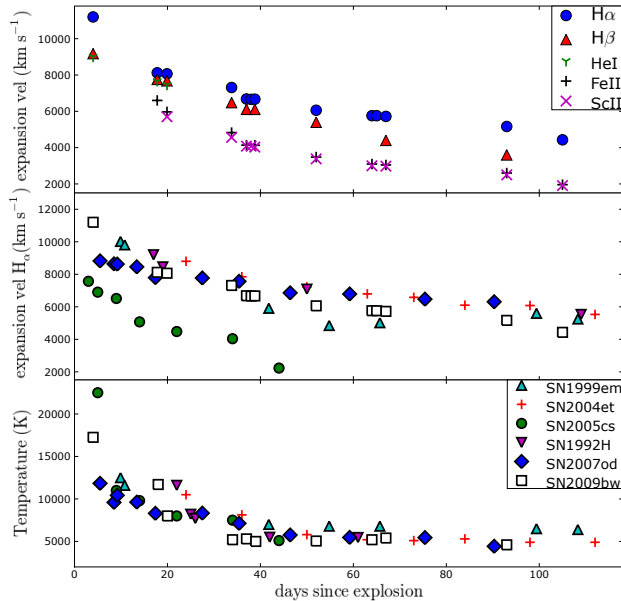
3.3 Expansion velocity and temperature

The photospheric expansion velocities of Hα, Hβ, He I λ5876, Fe II λ5169 and Sc II λ6246 are reported in Tab. 9 and plotted in Fig. 11 (top panel). They have been derived through the minima of P-Cygni profiles. Error estimates have been derived from the scatter of several independent measurements. Hα is always the strongest line, and the derived velocities are systematically the largest. During the first 20d when He I λ5876 dominates over Na ID, the He I velocity is comparable with that of Hβ. The Fe II velocity, which is considered to be a good indicator for the photospheric velocity because of the small optical depth, is lower

Table 9. Observed blackbody temperature and expansion velocities in SN 2009bw. For the Balmer lines the velocities were measured on the red wing component.

JD +2400000	Phase* (days)	T (K)	v(H_α) (km s^{-1})	v(H_β) (km s^{-1})	v(He I) (km s^{-1})	v(Fe II) (km s^{-1})	v(Sc II) (km s^{-1})
54920.5	4.0	17250 ± 1000	11200 ± 2000	9180 ± 1000	9000 ± 500		
54934.3	17.8	11700 ± 700	8122 ± 200	7760 ± 120	7658 ± 122	6600 ± 400	
54936.3	19.8	8000 ± 500	8067 ± 80	7682 ± 150	7454 ± 100	5970 ± 400	5700 ± 600
54950.3	33.8	5200 ± 400	7313 ± 300	6480 ± 300		4828 ± 300	4560 ± 200
54953.5	37.0	5300 ± 500	6680 ± 200	6110 ± 200		4138 ± 100	4080 ± 140
54954.5	38.0	5200 ± 400	6660 ± 300				4080 ± 140
54955.3	39.0	5000 ± 500	6670 ± 200	6109 ± 130		4130 ± 100	4030 ± 200
54968.5	52.0	5050 ± 250	6060 ± 60	5400 ± 400		3480 ± 100	3380 ± 120
54980.5	64.0	5200 ± 300	5760 ± 300			3097 ± 80	3000 ± 200
54981.5	65.0	5250 ± 250	5759 ± 180			3000 ± 200	
54983.5	67.0	5400 ± 300	5720 ± 300	4400 ± 230		3045 ± 150	2980 ± 200
54509.5	93.0	4600 ± 200	5165 ± 150	3600 ± 180		2600 ± 300	2500 ± 150
55021.5	105.0		4430 ± 100			1960 ± 300	1910 ± 110

* with respect to the explosion epoch (JD 2454916.5)

Figure 11. Top: expansion velocity of Hα, Hβ, HeI λ5876, FeII λ5169 and Sc II λ6246 measured from the minima of P-Cygni profiles. Middle: comparison of the Hα velocity of SN 2009bw with those of other SNe II. Bottom: Evolution of the continuum temperature of SNe 2009bw, 2007od, 1999em, 2004et, 2005cs, 1992H.

than those of H and He, reaching 3000 km s^{-1} at about two months. Sc II is also a good indicator of the photospheric velocity and indeed its velocity is very close to that of Fe II, supporting the identification of the lines of both ions.

In Fig. 11 (middle) we compare the Hα velocity evolution of SN 2009bw with those of other type IIP SNe. The velocity of SN 2009bw in the first two months is close to those of type IIP as SNe 1999em, 2004et, 1992H and 2007od, and higher than that of SN 2005cs which is known to have an exceptionally slow photospheric expansion. Afterwards, the photospheric velocity of SN 2009bw slowly decreases, showing a trend that is slightly different from that of other

type II SNe. This may be attributed to the presence of a moderate/low-density CSM that changes the shape of the absorption profile of Hα (see Sect. 5).

In Fig. 11 (bottom) the evolution of the photospheric temperature, derived from a blackbody fit to the spectral continuum, is shown and is compared to those of the reference sample. We already mentioned that the first spectrum of SN 2009bw is quite blue, indicating high black-body temperatures (1.7±0.1 x 10^4 K). The temperature remains high also at the second epoch (∼18d). Nevertheless, the temperature evolution of SN 2009bw is normal and not so different from those of the other SNe in the sample: its ejecta is probably hotter in the first month (similar to SN 1992H) and marginally cooler than average from the plateau onward.

4 EXPLOSION AND PROGENITOR PARAMETERS

We have inferred the physical properties of the SN 2009bw progenitor (namely, the ejected mass, the progenitor radius, the explosion energy) by performing a model/data comparison based on a simultaneous χ^2 fit of the main observables (i.e. the bolometric light curve, the evolution of line velocities and the continuum temperature at the photosphere), using the same procedure adopted for SN 2007od in Inserra et al. (2011).

According to this procedure, we employ two codes, the semi-analytic code presented in Zampieri et al. (2003) to perform a preparatory study in order to constrain the parameter space, and a new code which includes an accurate treatment of the radiative transfer and radiation hydrodynamics (Pumo, Zampieri, & Turatto 2010; Pumo & Zampieri 2011), to narrower grid of models.

The application of these two codes is appropriate if the SN emission is dominated by the expanding ejecta. For SN 2009bw the contamination from interaction may in part affect the observables (cfr. Sect. 5) and the possibility to reproduce the observed features is to be taken with caution. However, since there is no evidence that the ejecta–CSM in-
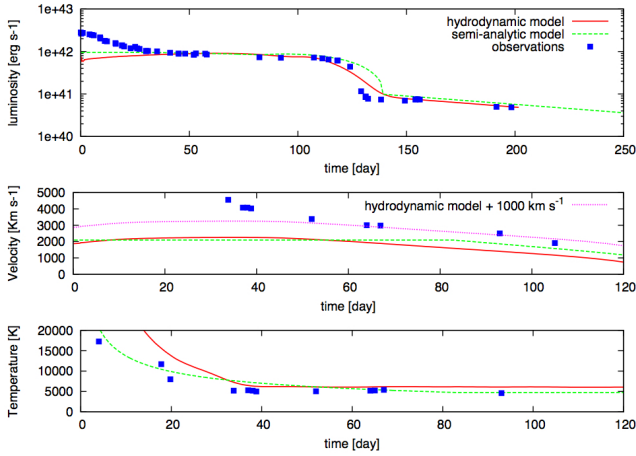
Figure 12. Comparison of the evolution of the main observables of SN 2009bw with the best-fit models computed with the semi-analytic code (total energy ~ 0.3 foe, initial radius 3.6×10^{13} cm, envelope mass 8.3 $M_\odot$) and with the relativistic, radiation-hydrodynamics code (total energy ~ 0.3 foe, initial radius 7×10^{13} cm, envelope mass 12 $M_\odot$). Top, middle, and bottom panels show the bolometric light curve, the photospheric velocity, and the photospheric temperature as a function of time, respectively. To estimate the photospheric velocity from the observations, we used the value inferred from the Sc II lines (often considered to be a good tracer of the photosphere velocity in type II SNe). The dotted-purple line is the radiation-hydrodynamics model shifted by 1000 $\mathrm{km\,s^{-1}}$ to reproduce the later epochs of data (see text).

teraction is a strong effect during most of the post-explosive evolution, our modeling can still be applied to SN 2009bw, returning a reliable estimate of the physical parameters of the explosion that can be useful to characterize its progenitor.

The distance and shock breakout epoch are taken from Tab. 6. In order to evaluate the uvoir (from optical to NIR) bolometric luminosity, we further assume that the SN has the same SED evolution as SN 1999em and hence

$$L_{09bw} = (L_{99em}/L_{99em}^{UBVRI}) \times L_{09bw}^{UBVRI},$$

where L_{09bw}/L_{99em} and $L_{09bw}^{UBVRI}/L_{99em}^{UBVRI}$ are the uvoir bolometric and quasi bolometric luminosity of SN 2009bw and SN 1999em (Elmhamdi et al. 2003), respectively.

Assuming a ^{56}Ni mass of 0.022 $M_\odot$ (see Sect. 2.4), the best fits of the semi-analytic and numerical models are in fair agreement and return values for the total (kinetic plus thermal) energy of ~ 0.3 foe, an initial radius of $3.6 - 7 \times 10^{13}$ cm, and an envelope mass of $8.3 - 12$ $M_\odot$.

The agreement between our modeling and the observed luminosity and temperature evolution is reasonably good, except at early epochs ($\lesssim 33$d, cfr. Fig. 12). These discrepancies may in part be caused by some ejecta-CSM interaction (see discussion in Sect. 5), leading to an excess of the observed luminosity, and to the approximate initial density profile used in our simulations, that does not reproduce correctly the radial profile of the outermost high-velocity (HV) shell of the ejecta formed after shock breakout (cfr. Pumo & Zampieri 2011)

During the entire photospheric phase the best fit of the velocity is unsatisfactory. This is unusual for the Pumo and Zampieri code that has proved to work well for standard

SNe II, reinforcing the idea that for SN 2009bw the ejecta–CSM interaction could be at work. Indeed the discrepancies between the simulated photospheric velocity and the data could be related to the interaction creating of a pseudo-photosphere at a larger radius, hence at a higher velocity ($\Delta v \sim 1000$ $\mathrm{km\,s^{-1}}$), than expected by the model (cfr. Fig. 12, middle panel, purple-dotted line). This effect has been found in luminous and interacting SNe as shown by Agnoletto et al. (2009).

The model parameters reported above are consistent with both a super-asymptotic giant branch (SAGB) star, with a mass close to the upper limit of this class, and a progenitor of a small Fe core collapse SN with a mass close to the lower limit. They are reliable progenitors even if, through the first one is difficult to explain the amount of ^{56}Ni (e.g. Wanajo et al. 2009), instead the second one poorly explains the mass loss and the probable mixing related to the CNO elements (e.g. Maeder & Meynet 2008). However, in both scenarios the progenitors are expected to have a radius of $\sim$1000 $R_\odot$ (Garcia-Berro & Iben 1994; Ritossa, García-Berro, & Iben 1999; Woosley, Heger, & Weaver 2002) and hence to fall into the red supergiant (RSG) category (200 $R_\odot < R < 1500$ $R_\odot$).

5 DISCUSSION

In the previous Sections we have presented and discussed the photometric and spectroscopic data of SN 2009bw in UGC 2890 from the photospheric to the early nebular stages.

The analysis reported in Sect. 2.4 indicates that SN 2009bw was a relatively luminous SN IIP with a peak magnitude similar to that of SN 1992H ($M_V = -17.67$) and an extended plateau in V, R and I. The duration of the plateau suggests an envelope mass not dissimilar from that of standard SNe IIP such as SN 1999em, that in the nebular phase shows strong similarity with SN 2009bw both in photometry and spectroscopy. The rise to maximum seems relatively slow for a SN IIP (~ 8d) and the peak somehow broad. The light curves show a steep but shallow drop of $\sim$2.2 mag in $\sim$13d from the end of the plateau to the tail. The tail is flat for the first couple of months, then declines with the canonical ^{56}Co decline rate of 0.98 mag/100d. The luminosity of the radioactive tail indicates an ejected mass of ^{56}Ni of M(^{56}Ni)~ 2.2x10^{-2} $M_\odot$ (cfr. Tab. 6), which is comparable to that estimated for SN 1999em (Elmhamdi et al. 2003).

The spectral evolution is quite similar to that observed in canonical SNe IIP, although an unidentified, broad feature is present in the first photospheric spectrum, at about 4600Å. A plausible interpretation is that the feature is due to emission emerging in a region of low opacity.

The host galaxy has been classified as an highly inclined peculiar Magellanic Spiral (Sdm pec:). In the spectra an unresolved component due to an underlying H II region is clearly visible. A reasonable assumption is to consider the SN has the same metallicity of the H II region. From the spectra obtained at Calar Alto on Sept. 4 and at TNG on Oct. 11, 2009, we have measured the N2 and (only for the CAHA spectrum) the O3N2 indices (Pettini & Pagel 2004) of the H II region extracted close to the SN along the slit of the spectrograph. The average relations of Pettini & Pagel

(2004) then provide the O abundances which turn out to be $12+\log(O/H) = 8.66 \pm 0.06 \pm 0.41$ (where the first error is statistical and the second one is the 95% spread of the N2 index calibration relation). While the projected distance from the galaxy nucleus is relatively small (2.4 kpc) we were unable to determine the deprojected one because of the very high inclination (i= 90°) of the parent galaxy (Sect. 1). Pilyugin, Vílchez, & Contini (2004) have shown that the central oxygen abundances of spiral galaxies is typically $8.3 < [12+\log O/H] < 9.1$, similar to solar abundance (8.69, Asplund et al. 2009). Therefore, the estimated progenitor metallicity is close to solar and in line with the expected metallicity at the position inside the parent galaxy.

No information is available in the literature about the X-ray and radio emission of the SN. An observation (8 ksec) with Swift-XRT has been obtained generating a single combined and astrometrically-corrected event file. In an aperture of 9 XRT pixels ($\sim$21") centered at the position of SN 2009bw we obtained a limit on total source counts of n < 5. Considering a column density of $N_H = 1.9 \times 10^{21}$ cm^{-2} (Dickey & Lockman 1990; Predehl & Schmitt 1995) we have measured an upper limit to the X-ray flux (over the energy range 0.3–10 keV) 7.9×10^{-14} erg cm^{-2} s^{-1} corresponding to upper limits of the X-ray luminosity of $L_X < 3.77 \times 10^{39}$ erg s^{-1} (thermal bremsstrahlung model with kT = 10 kev) and 1.6×10^{-13} erg cm^{-2} s^{-1} corresponding to $L_X < 7.65 \times 10^{39}$ erg s^{-1} (power law model with photon index Γ=1.7). These X-ray luminosity upper limits do not preclude the possibility of a weak interaction as in SN IIP 1999em. Indeed, SN 1999em was detected at a similar phase at fainter flux ($\sim 10^{-14}$ erg cm^{-2} s^{-1} in both the 2-8 keV and 0.4–2 keV bands) thanks to the superior performance of Chandra. The corresponding X-ray luminosity is one order of magnitude smaller than our upper limit (L_X(99em) $\sim 2 \times 10^{38}$ erg s^{-1}, in the 0.4-8 keV range, Pooley et al. 2002) because of the much shorter distance.

However, some observational evidence point in favour of weak CSM interaction in SN 2009bw. The spectral line contrast in the early photospheric period seems smaller than in other SNe IIP (cfr. panel a & b of Fig. 8), as expected in the case of resonance scattering due to external illumination of the line forming region by CSM interaction (the so called toplighting, Branch et al. 2000). In addition, the spectra show the presence of secondary absorptions in the H Balmer lines that we interpret as HV features. The right panel of Fig. 13 shows the presence of a blue Hα component at about 7300 km s^{-1} that does not evolve with time, and a redder component decreasing progressively in velocity in analogy with other photospheric lines measured in Fig. 11. Careful analysis of Hβ (left panel of Fig. 13) shows the same bluer non-evolving component as well as the photospheric one, despite the optical depth of the line being smaller than that of Hα. Blue secondary features, constant with time, were also identified in SNe 1999em and 2004dj by Chugai, Chevalier, & Utrobin (2007). According to these authors, the lines are HV components of the Balmer lines. Their analysis shows that the interaction of the ejecta of a SN IIP with an average RSG wind can be detected during the photospheric stage through the emergence of absorptions (shoulders) on the blue wings of the undisturbed H lines due to enhanced excitation of the outer unshocked ejecta. In SN 2009bw the unshocked layers producing the HV absorptions are at about

7300 km s^{-1}, while the photospheric absorption moves from 6700 to 4400 km s^{-1} between the early and the very late photospheric phase (day 37 to 105). Chugai, Chevalier, & Utrobin (2007) also predicted that during the late photospheric phase the physical conditions in the cool dense shell (CDS) behind the reverse shock allow the formation of a notch, a smaller and narrower absorption, at the fastest edge of the line, and recovered it in the spectra of SN 2004dj. We clearly see this notch with similar intensity and position in SN 2009bw starting from 2 months past explosion, both for Hα and Hβ. The line position is compatible with the expected position of Fe II lines at the earliest epoch, but the fact that it does not evolve disfavors such an identification.

Only one NIR spectrum is available, at an epoch (21d) when the two components of the Balmer lines are blended. The NIR spectrum shows a strong feature at about 10500Å. If we identify it as He I λ10830, the expansion velocity turns out to be larger (v$_{He} \sim$ 10000 km s^{-1}) than that of He I λ5876 (which has no sign of a photospheric component), and larger than that of the HV Balmer components. A NIR spectrum of SN 1999em at a similar epoch is available (Elmhamdi et al. 2003), showing an absorption identified by Chugai, Chevalier, & Utrobin (2007) as HV He I at a velocity which was marginally higher than those of H and without a photospheric component. The alternative identification with Mg II λ10926 or Fe II λ10862 would imply even larger velocities. In conclusion, the close similarity with the features observed in SN 1999em and SN 2004dj and well modeled by Chugai, Chevalier, & Utrobin (2007), leads us to favour the HV Balmer component scenario. Line profile models suggest a typical red supergiant wind with a density of $w = \dot{M}_{-6}/u_{10} \sim 1$, i.e. $\dot{M} \sim 10^{-6}$ M$_\odot$ yr^{-1}, similar to those of SNe 1999em and 2004dj (Chugai, Chevalier, & Utrobin 2007), or even higher. Assuming a typical duration of 10^6 yr, the mass lost by the progenitor star is about 1M$_\odot$.

Late photospheric spectra of SN 2009bw show absorption features of CNO elements (see Sect. 3.2), indicating a potentially enhanced mixing with deep layers, which may be an indicators of a high metallicity envelope, prone to enhanced mass loss. Similar features in the red part of the optical spectra, related to the CNO elements, have been seen also in SN 1999em (Pastorello 2003) and SN 1995V (Fassia et al. 1998), both presenting signatures of weak CSM interaction (Pooley et al. 2002; Chugai, Chevalier, & Utrobin 2007). The presence of C in the photospheric spectra rises the possibility of CO molecules formation, that with their rotation-vibration states are a powerful coolant and are a necessary condition for dust condensation in the ejecta. Indeed SN 1999em showed both C in the photospheric spectra and dust formation in the inner ejecta after t$\sim$500d (Elmhamdi et al. 2003). In SN 2009bw there is no direct evidence of dust formation (neither photometric nor spectroscopic) though the last two points of the light curves, affected by large uncertainties, may indicate a steepening of the decline with respect to the slope of ^{56}Co.

Moriya et al. (2011) studied the interaction between SN ejecta and the CSM around RSGs. They showed that, if the temperature and the CSM density are high enough, the CSM around SNe IIP becomes optically thick and the effective photosphere forms at large radii inside the CSM. The interaction-powered phase is characterized by light curves with broad peaks, flat plateau brighter for large $\dot{M}$ and
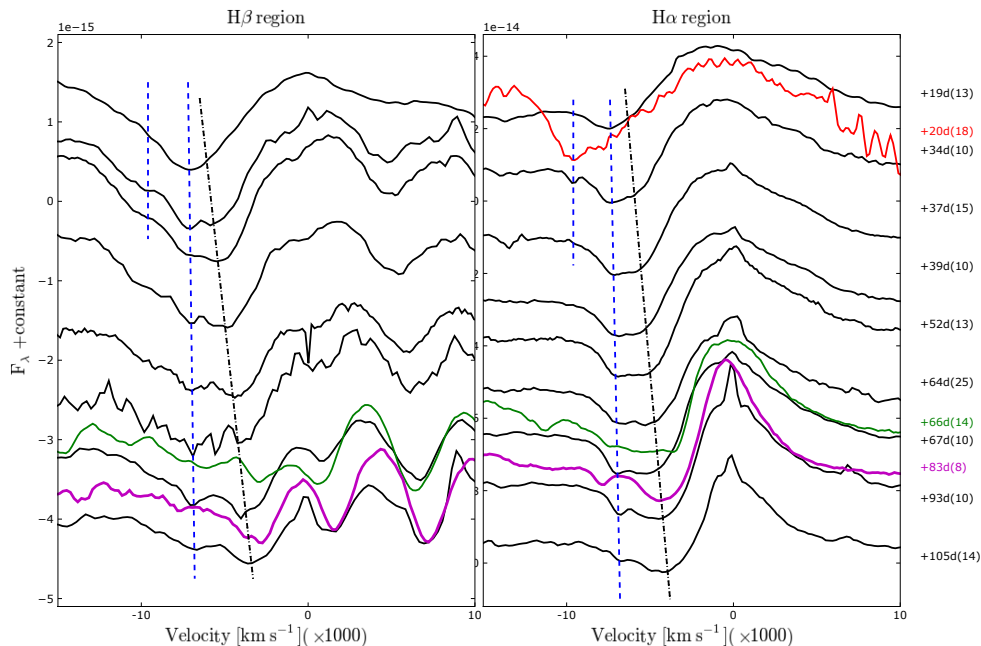
Figure 13. Zoom of the Hβ (left-hand panel) and Hα (right-hand panel) spectral regions during the plateau phase of SN 2009bw. The x-axes are in expansion velocity coordinates with respect to the rest-frame positions of the lines. In order to guide the eye, two black dash-dotted lines are drawn in the spectra corresponding expansion velocities. Similarly two blue dashed lines follow the HV features of the Balmer lines. The red spectrum (+20d) shows the NIR He I feature centered at 10830Å. We have also reported the spectra of SN 2004dj (purple, +83d) and SN 1999em (green, +66d) for comparison.

longer for an extended CSM. The observed expansion velocity at early times is expected to be that of the CSM, then turning to typical SN values when the photosphere recedes into the ejecta. In particular, the early light curves of very bright SNe IIP can be interpreted in terms of interaction with a dense CSM produced by a mass loss at a rate larger than ∼ 10^{-4} M$_\odot$ yr^{-1}. The interaction ejecta–CSM applied to the luminous SN 2009kf (Botticella et al. 2010) satisfactorily explained the early multicolor light curves, but failed in explaining the late behaviour and the kinematics, possibly because it was an energetic explosion with large ^{56}Ni production. We have seen above that the line profiles of SN 2009bw would point toward a normal RSG wind with a low value of $\dot{M}$, which is of the order of ∼10^{-6} M$_\odot$ yr^{-1} (or marginally higher). This is much smaller than the values expected to significantly increase the luminosity. In addition, we have not detected any unusual behaviour in the velocity evolution. Nevertheless, we cannot exclude that a fraction of the observed luminosity during the plateau of SN 2009bw might be due to the transformation of ejecta kinetic energy into radiation via interaction with the CSM. As already highlighted in Sect. 4, this may explain why, differently from our previous experience (Pumo & Zampieri 2011; Inserra et al. 2011; Pastorello et al. 2011) where the main observables are simultaneously reproduced by our modelling, here we fail to reproduce the kinetic evolution, whilst both the bolometric light curve (cfr. Fig. 5) and the spectra in the nebular phase (cfr. panel d of Fig. 8) are standard, and very similar to those of SN 1999em.

As reported in Sect. 4, the ejecta mass is ∼ 8 − 12 M$_\odot$. Accounting for a compact remnant (NS) of ∼ 1.6 M$_\odot$ and about 1 M$_\odot$ of mass loss, the initial mass of the progeni-

tor is of the order of 11 − 15 M$_\odot$, comparable with that of massive SAGB stars or a low mass Fe CC-SN progenitor. Despite that, we want to notice that the weak intensity of [O I] λλ6300−6363 may be inconsistent with the progenitor mass (too high for the intensity observed), but the similarity between the late spectra of SN 2009bw and SN 1999em and the previous modelling case of the weak interacting SN 2007od (Inserra et al. 2011), are in favour of this mass range.

6 CONCLUSIONS

In this paper we show, for the first time, photospheric and spectroscopic data of SN 2009bw. The peak (M$_R$ = −17.82) and the plateau (M$_R$ = −17.37) magnitudes allow us to accommodate this SN in the small sample of the brightest type IIP SNe. The fast jump from the plateau phase to the nebular tail (∼2.2 mag in 13d, unusual among bright type II SNe), the proof of the presence of CNO elements in the photospheric spectra and the detection of HV features in the Balmer lines during the recombination phase suggesting an early interaction, make this object atypical in the context of type IIP events.

The well sampled light curve of SN 2009bw reaches a luminous plateau at M$_R$ = −17.37 between ∼50d and ∼100d. This is a standard duration for the plateau phase in SNe IIP. The high photospheric luminosity contrasts with the moderate luminosity of the tail (similar to that of SN 1999em). The post-plateau decline is relatively rapid, resembles that of SN 1986L (although this object has not been well studied; Hamuy 2001) and has been well monitored, making this constraint rather solid. The remarkable magnitude drop is

analogous to that observed in faint SNe IIP (Pastorello et al. 2004). The bolometric light curve tail follows the slope expected if the main energy source is the decay of ^{56}Co into ^{56}Fe. The ^{56}Ni mass derived from the quasi bolometric (U to I) light curve is M(^{56}Ni)$\sim$0.022 M$_\odot$, similar to that of the prototypical SN IIP 1999em. If instead, the ^{56}Ni mass is estimated from the post plateau drop with a steepness $S = 0.57$, M(^{56}Ni)$\sim$0.002 M$_\odot$ is obtained. This value suggests that for SN 2009bw the anti-correlation between the steepness function and ^{56}Ni mass does not work in this case, possibly masked by the presence of other effects, such as CSM interaction or dust formation.

Thanks to detailed synthetical spectral computed using the LTE code `SYNOW`, we noted the presence of the Si II $\lambda 6355$ feature in the early spectra, and of CNO element lines in the plateau spectra. Highly ionized C and N features have been tentatively identified in our first spectrum as being responsible for the prominent blend at 4600Å. HV line components of the Balmer series (Hα and Hβ at v$\sim$7300 km s^{-1}) have been clearly identified in the plateau spectra from $\sim$37d onwards, though they become more prominent from day 52 to day 105. These lines, similar to those observed in SNe 2004dj and 1999em (Chugai, Chevalier, & Utrobin 2007), suggest an early interaction with a barely dense CSM. Based on the similitudes between SN 2009bw and SN 1999em, the absence of remarkable changes in the light curve (see Moriya et al. 2011) and the early line velocity evolution, we roughly estimate the progenitor's mass loss to be in the range $10^{-6} < \dot{M} < 10^{-4}$ M$_\odot$ yr^{-1}, even though it is probably closer to the lower limit. Assuming a typical duration of 10^6 yr, the mass lost by the progenitor star is 1M$_\odot$. Our latest spectra have been useful to estimate the N2 and O3N2 indices (Pettini & Pagel 2004), revealing an average oxygen abundance of 12+log(O/H)$\sim$8.66, which corresponds to about solar metallicity.

The presence of CNO elements, the similarities with SN 1999em at late phase and the increased slope of the radioactive tail as suggested by the last two photometric points (although with a large uncertainty) might indicate late dust formation in the inner ejecta.

Modelling gives to us an ejecta mass of $8 - 12$ M$_\odot$, corresponding to an initial mass of the progenitor of the order of $11 - 15$ M$_\odot$. This is consistent with a RSG, which could be both with a massive SAGB star or a star exploded as small Fe CC-SN, explaining the most part of the peculiarities (early interaction, ^{56}Ni mass and CNO elements) of this object. The unsatisfactory fit of the velocity during the entire photospheric phase strengthens the idea of ejecta–CSM interaction. In fact, the interaction could have caused the formation of a pseudo-photosphere at a radius larger than expected by the model.

SN 2009bw shows some properties in common with both luminous and standard SNe IIP. Our study has revealed: - HV features as in SNe 1999em, 2004dj and 2007od; - ejecta-CSM interaction ongoing during the entire photospheric phase, reinforcing the idea that interaction can be significant also for SNe IIP; - and the presence of CNO elements seen in few SNe IIP. Luminous SNe IIP with weak CSM interaction may bridge the gap between normal SNe IIP and interaction dominated SNe IIn, and may thus be helpful to create a united scheme of all CC explosions.

REFERENCES

Agnoletto I., et al., 2009, ApJ, 691, 1348
Asplund M., Grevesse N., Sauval A. J., Scott P., 2009, ARA&A, 47, 481
Arnett W. D., Bahcall J. N., Kirshner R. P., Woosley S. E., 1989, ARA&A, 27, 629
Arnett W. D., 1996, Supernovae and Nucleosynthesis, Princeton University Press, Princeton
Barbon R., Ciatti F., Rosino L., 1979, A&A, 72, 287
Baron E., et al., 2000, ApJ, 545, 444
Botticella M. T., et al., 2010, ApJ, 717, L52
Branch D., Jeffery D. J., Blaylock M., Hatano K., 2000, PASP, 112, 217
Cardelli J. A., Clayton G. C., Mathis J. S., 1989, ApJ, 345, 245
Cappellaro E., Mazzali P. A., Benetti S., Danziger I. J., Turatto M., della Valle M., Patat F., 1997, A&A, 328, 203
Chugai N. N., Chevalier R. A., Utrobin V. P., 2007, ApJ, 662, 1136
Clocchiatti A., et al., 1996, AJ, 111, 1286
Dessart L., Hillier D. J., 2005, A&A, 437, 667
Dickey J. M., Lockman F. J., 1990, ARA&A, 28, 215
Elmhamdi A., et al., 2003, MNRAS, 338, 939
Elmhamdi A., Chugai N. N., Danziger I. J., 2003, A&A, 404, 1077

Fassia A., Meikle W. P. S., Geballe T. R., Walton N. A., Pollacco D. L., Rutten R. G. M., Tinney C., 1998, MNRAS, 299, 150

Fassia A., et al., 2001, MNRAS, 325, 907

Garcia-Berro E., Iben I., 1994, ApJ, 434, 306

Fisher A., 2000, PhD thesis, Univ. Oklahoma

Hamuy M. A., 2001, PhDT, The University of Ariziona

Hamuy M., 2003, ApJ, 582, 905

Harutyunyan A. H., et al., 2008, A&A, 488, 383

Heger A., Fryer C. L., Woosley S. E., Langer N., Hartmann D. H., 2003, ApJ, 591, 288

Inserra C., et al., 2011, MNRAS, 417, 261

Landolt A. U., 1992, AJ, 104, 340

Maeder A., Meynet G., 2008, ASPC, 388, 3

Maguire K., et al., 2010, MNRAS, 404, 981

Moriya T., Tominaga N., Blinnikov S. I., Baklanov P. V., Sorokina E. I., 2011, MNRAS, 415, 199

Mould J. R., et al., 2000, ApJ, 529, 786

Nissinen M., Heikkinen E.P, Hentunen V.-P., 2009, CBET, 1743, 1

Pastorello A., 2003, PhD. thesis, Univ. Padova

Pastorello A., et al., 2004, MNRAS, 347,74

Pastorello A., et al., 2006, MNRAS, 370,1752

Pastorello A., et al., 2009, MNRAS, 394, 2266

Pastorello A., et al., 2010, ApJ, 724, L16

Pastorello A., et al., 2011, arXiv, arXiv:1111.2497

Patat F., Barbon R., Cappellaro E., Turatto M., 1994, A&A, 282, 731

Pettini M., Pagel B. E. J., 2004, MNRAS, 348, L59

Pilyugin L. S., Vílchez J. M., Contini T., 2004, A&A, 425, 849

Poole T. S., et al., 2008, MNRAS, 383, 627

Pooley D., et al., 2002, ApJ, 572, 932

Poznanski D., Ganeshalingam M., Silverman J. M., Filippenko A. V., 2011, MNRAS, 415, L81

Predehl P., Schmitt J. H. M. M., 1995, A&A, 293, 889

Pumo M. L., et al., 2009, ApJ, 705, L138

Pumo M. L., Zampieri L., Turatto M., 2010, MSAIS, 14, 123

Pumo M. L., Zampieri L., 2011, ApJ, 741, 41

Quimby R. M., Wheeler J. C., Höflich P., Akerlof C. W., Brown P. J., Rykoff E. S., 2007, ApJ, 666, 1093

Quimby R. M., et al., 2011, Nature, 474, 487

Richardson D., Branch D., Casebeer D., Millard J., Thomas R. C., Baron E., 2002, AJ, 123, 745

Ritossa C., García-Berro E., Iben I., Jr., 1999, ApJ, 515, 381

Rutten, R.J., 2003, Radiative Transfer in Stellar Atmospheres, Utrecht University lecture notes, 8th edition

Schmidt B. P., et al., 1993, AJ, 105, 2236

Schlegel E. M., 1990, MNRAS, 244, 269

Schlegel D. J., Finkbeiner D. P., Davis M., 1998, ApJ, 500, 525

Smartt S. J., Eldridge J. J., Crockett R. M., Maund J. R., 2009, MNRAS, 395, 1409

Smartt S. J., 2009, ARA&A, 47, 63

Sollerman J., Cumming R. J., Lundqvist P., 1998, ApJ, 493, 933

Stanishev V., Adamo A., Micheva G., 2009, CBET, 1746, 1

Suntzeff N. B., Bouchet P., 1990, AJ, 99, 650

Tsamis Y. G., Barlow M. J., Liu X.-W., Danziger I. J., Storey P. J., 2003, MNRAS, 338, 687

Tully R. B., Rizzi L., Shaya E. J., Courtois H. M., Makarov D. I., Jacobs B. A., 2009, AJ, 138, 323

Turatto M., Cappellaro E., Barbon R., della Valle M., Ortolani S., Rosino L., 1990, AJ, 100, 771

Turatto M., Benetti S., Cappellaro E., 2003, in Hillebrandt W., Leibundgut B., eds, ESO Astrophys. Symp. Vol. XVII, From Twilight to Highlight: the Physics of Supernovae. Springer, Berlin , p. 200

Zampieri L., Pastorello A., Turatto M., Cappellaro E., Benetti S., Altavilla G., Mazzali P., Hamuy M., 2003, MNRAS, 338, 711

Wanajo S., Nomoto K., Janka H.-T., Kitaura F. S., Müller B., 2009, ApJ, 695, 208

Woosley S. E., Hartmann D., Pinto P. A., 1989, ApJ, 346, 395

Woosley S. E., Heger A., Weaver T. A., 2002, RvMP, 74, 1015